MORPHOLOGY STUDY OF STRUCTURE I METHANE HYDRATE FORMATION ON WATER DROPLETS IN THE PRESENCE OF KINETIC INHIBITORS

by

Lindsay Dianne Lessard

Department of Chemical Engineering

McGill University
Montréal, Québec, Canada

September 2006

A thesis submitted to the Faculty of Graduate Studies and Research in partial fulfillment of the requirements of the Degree of Master's of Engineering

Your file Votre référence
ISBN: 978-0-494-28604-3
Our file Notre référence
ISBN: 978-0-494-28604-3

ABSTRACT

Gas hydrates are non-stoichiometric crystalline compounds that occur when water molecules hydrogen bond to form cavities which can be stabilized by the presence of a guest molecule such as a gas or volatile liquid. Hydrates have been problematic in the oil and gas industry for several years as they may block pipelines and damage equipment. It is therefore of great interest to find environmentally safe inhibitors which can prevent hydrates from forming or from growing large enough to block pipelines.

The purpose of my study was to observe the effect of kinetic inhibitors on the morphology of methane structure I hydrate using a high pressure crystallizer. Two kinetic inhibitors were studied, poly(VP/VC), a lactam ring copolymer, and antifreeze protein.

Experiments were carried out on droplets with and without memory at pressures ranging from 5000 kPa to 10,000 kPa. There was no evident trend in induction times since nucleation is a stochastic process. Surface coverage time of each droplet was measured and found to be fastest on the water droplet followed by that of the poly(VP/VC) droplet and finally the AFP droplet, confirming that the two kinetic inhibitors studied were in fact effective at inhibiting hydrate growth. Since hydrate growth, unlike nucleation, can reliably be measured we can definitively conclude that AFP has a greater kinetic inhibiting effect on hydrate growth.

During hydrate decomposition, it was observed in all experiments that the water droplet decomposed first followed by the poly(VP/VC) droplet and the AFP droplet. It is proposed that since the polymer chains and protein molecules bind to the hydrate crystals, this reduces the surface area of hydrate skin exposed, slowing the rate of decomposition.

SOMMAIRE

Les hydrates de gaz sont des composés cristallins non stœchiométriques qui se forment lorsque des molécules d'eau s'arrangent pour créer des cavités. Ces cavités peuvent ensuite être occupées par des molécules simples tel le méthane. Les hydrates sont problématiques dans l'industrie du pétrole parce qu'ils peuvent bloquer les oléoducs et endommager l'équipement. Il est donc important de trouver un moyen pour prévenir leur formation et leur croissance.

Le but de la présente recherche était d'observer l'effet d'inhibiteurs cinétiques sur la morphologie d'hydrates de méthane de structure I dans un réacteur à haute pression. Deux inhibiteurs cinétiques ont été étudiés: un copolymère composé de chaînes de lactames et une protéine antigel.

Les expériences ont été exécutées sur des gouttelettes d'eau avec et sans mémoire à des pressions entre 5,000 kPa et 10,000 kPa. Il n'y avait pas de tendance évidente dans les temps de nucléation puisque la nucléation est un phénomène stochastique. Le temps pris pour couvrir complètement une gouttelette d'hydrates a été mesuré. La formation était plus rapide sur la gouttelette d'eau, suivie de celle avec le copolymère et finalement celle avec la protéine antigel. Ceci confirme que les deux inhibiteurs cinétiques étudiés parviennent à limiter la croissance des hydrates de gaz. Puisque la croissance des hydrates de gaz, contrairement à la nucléation, peut être mesurée, les résultats

démontrent que la présence de protéines antigel limite la croissance des hydrates de gazde façon plus efficace que la présence du copolymère étudié.

Pendant la décomposition de la couche d'hydrate sur les gouttelettes, on a observé dans toutes les expériences que la couche sur la gouttelette d'eau se décomposait en

premier, suivie de la couche sur la gouttelette contenant le copolymère et finalement la couche sur la gouttelette contenant la protéine antigel. Il a été postulé que, puisque les chaînes polymériques et les molécules de protéines s'attachent aux cristaux d'hydrate, la superficie exposée des hydrates est réduite, ce qui ralenti la vitesse de décomposition.

ACKNOWLEDGEMENTS

I would like to thank Professor Servio for his guidance throughout the course of my Master's project. I think he set a record for being the fastest reviser in the department thanks to my strict deadlines.

These last two years would not have been the same without the lab group...thanks to (in no particular order) Juan, Naomi, Jason, Shadi, Sébastien, André, Yeshai, Rakan, Hal and Jessica. John, you were a patient office mate, full of good advice and always willing to help out with any problems I had in and outside the lab. You have helped make my time at McGill a very memorable experience. I haven't forgotten about the rest of the 7th floor crew! Good luck with all your lab work, thesis writing, presentations, etc.....trust me, it's rewarding in the end.

Many thanks to Louise, Emily, Melanie, Alain, Charles and Roberto. I am also grateful to Frank for his useful advice and helpful ideas over the course of my research project.

My family has been a huge support outside the Wonderful Wong. Thank you Mom and Dad for pushing me throughout my entire time at McGill University. I'm grateful for everything you've done for me! Thanks to Meg, Nadine and Sarah for being wonderful sisters, through good times and bad.

Fred, your advice has been fantastic and much appreciated throughout the last two years. Who better to take advice from than someone who's been through it all? Bonne chance en médecine! You're going to be a great doctor. Love you!

TABLE OF CONTENTS

LIST OF FIGURES

LIST OF TABLES

1 INTRODUCTION

Gas hydrates, also known as clathrates, are non-stoichiometric crystalline compounds that occur when water molecules hydrogen bond in a network and form cavities. The hydrogen bonding of the water molecules forms a cage-like structure known as the host lattice which is thermodynamically unstable without the presence of a guest molecule such as a gas or volatile liquid. The only interactions between the host lattice and guest molecule are weak van der Waals forces which are necessary in order to stabilize the host lattice. There is no chemical reaction or bonding between the guest molecule and host lattice. Clathrate hydrate crystals can exist at temperatures above and below the normal freezing point of water (Englezos, 1993).

The properties of gas hydrates have intrigued many researchers, fueling studies in the fields of energy and the environment. Hydrates have been problematic in the oil and gas industry for several years. When water is transported with a hydrate forming gas or volatile liquid, under suitable temperature and pressure conditions, hydrates may form. Under similar circumstances, hydrates may block pipelines, damaging equipment such as pumps and compressors. It is therefore of great interest to find environmentally safe inhibitors which can prevent hydrates from forming or from growing large enough to block pipelines (Hammerschmidt, 1934).

In the 1960's, the hypothesis of gas hydrates occurring naturally in the earth's crust was proven by Russian researchers (Makogon, 1972). They were found to consist mostly of methane and exist in extensive quantities within and below the permafrost zone and in sub sea sediment in the Arctic, the Antarctic and tropical and subtropical oceans (Englezos, 1993). They are viewed as a potential energy source, justifying efforts to

recover hydrates economically. It is estimated that the organic carbon present in methane hydrates in the seafloor and permafrost sediment store more energy than the organic carbon present in any other global fossil fuel reserves combined. In addition, unlike fossil fuels, which are rapidly being consumed, hydrate formation in the earth's crust is a continuous process.

There are environmental concerns linked to hydrate deposits. Trace atmospheric gases (TAG's) cause a temperature rise in the atmosphere. This rise in temperature can potentially cause decomposition of methane hydrates if increased above the three phase equilibrium temperature of methane hydrate. Methane has a global warming effect 21 times greater than that of carbon dioxide (Taylor, 1991). Since methane is such a strong greenhouse gas, releasing large amounts of it into the atmosphere can produce a runaway greenhouse effect. This means that increasing amounts of methane hydrate would continue to decompose due to global warming.

1.1 Historical Background of Gas Hydrates

Sir Humphry Davy first discovered hydrates in 1810 when he observed that chlorine gas in a solution of water would freeze at temperatures as high as 9.0 °C. Faraday confirmed this observation, suggesting that the compound consisted of approximately 1 part chlorine and 10 parts water. This established a basis for hydrate research, which has since developed into many different areas of specialization such as phase equilibrium, morphology and hydrate inhibition, among others (Hammerschmidt, 1934).

Initial research focused on determining which compounds formed hydrates in the presence of water. In 1934, Hammerschmidt discovered that hydrates could form and plug natural gas pipelines at temperatures above those at which water normally freezes, launching an industrial interest in hydrates. Much research is presently being devoted to the prediction and inhibition of hydrate formation. In 1965, the first discovery of *in situ* hydrates in the Siberian permafrost region by Makogon et al. launched widespread interest in recovering naturally forming gas hydrates in the field (Sloan, 1998a).

1.2 Clathrate Hydrate Structures

There are three naturally occurring hydrate structures: structure I, structure II and structure H. Hydrogen-bonded water molecules arrange themselves to form a cavity in the shape of a pentagonal dodecahedron, a polyhedron with 12 pentagonal faces (5^{12}). Structure I hydrate is formed when such cavities link together through the vertices, forming a second larger cavity, a polyhedron with 12 pentagonal faces and 2 hexagonal faces. A unit cell of structure I hydrate has 6 large cavities and 2 small cavities which are composed of 46 water molecules. Small molecules such as methane, ethane and carbon dioxide are suitable hosts for the cavities of a structure I hydrate, having a diameter ranging between 4.2 and 6.0 Å.

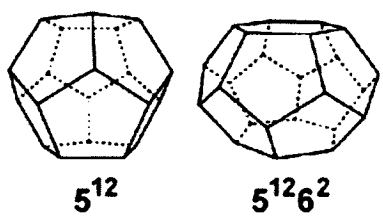

Figure 1.1: Cavities of structure I hydrate (http://www.pet.hw.ac.uk/research/hydrate/)

Structure II hydrate is formed when pentagonal dodecahedrons are linked through face sharing, thus creating a hexakaidecahedron, a polyhedron with 12 pentagonal faces and 4 hexagonal faces ($5^{12}6^4$). This cavity created is larger than the large cavity in structure I, but due to hydrogen bond bending, the small cavity in structure II is smaller than that of structure I. A unit cell of structure II hydrate consists of 136 water molecules having 16 small cavities and 8 large cavities. Molecules such as propane and iso-butane, which have a diameter ranging between 6 and 7 Å are examples of structure II forming compounds.

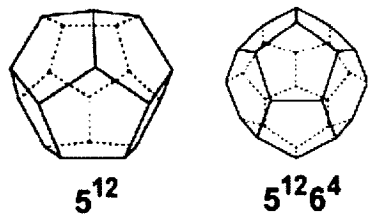

Figure 1.2: Cavities of structure II hydrate
(http://www.pet.hw.ac.uk/research/hydrate/)

Structure I and II hydrates do not necessarily need all cages filled in order to be thermodynamically stable. For example, a component that is too large to fill the smaller cavities but can fill the larger cavities in structure I and II hydrates can stabilize the structure. Very small molecules such as argon, krypton and nitrogen will fill the smaller cavities in structure II hydrate. Gas mixtures can form structure I or structure II hydrate by having different size molecules fill the small and large cavities.

Structure H, discovered by Ripmeester in 1987, is composed of three different cavities, two small and one large. Structure H differs not only from structure I and II in

terms of the numbers of different size cavities but also in terms of the number and sizes of guest molecules needed to stabilize the hydrate structure. The basic pentagonal dodecahedron cage (5^{12}) is one of the smaller cavities. A second small cavity consists of 3 square faces, 6 pentagonal faces and 3 hexagonal faces ($4^3 5^6 6^3$). The large cavity consists of 12 pentagonal and 8 hexagonal faces ($5^{12} 6^8$) and is the largest cavity of all three structures. Molecules with diameters up to 9 Å are estimated to fit in the large cavity of structure H hydrate. A unit cell contains one large and five small cavities at most and is made up of 34 water molecules. The shape and filling of the large cavity in structure H hydrate is important in terms of stability. Smaller molecules such as methane, xenon or hydrogen sulfide will occupy the small cages of structure H while larger molecules such as adamantine, cycloheptane or neohexane will occupy the larger cage.

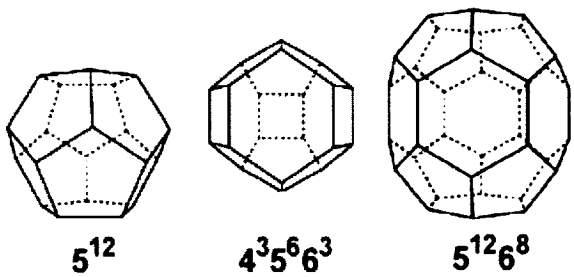

Figure 1.3: Cavities of structure H hydrate
(http://www.pet.hw.ac.uk/research/hydrate/)

1.3 Kinetics of Hydrate Formation

Hydrate formation, as in crystallization, can be sub-divided into nucleation and growth processes. There are two fundamental topics to be addressed when time is a consideration with respect to hydrate formation (Englezos, 1996). The first is induction time, the time required for a hydrate to reach a critical size nucleus. The second is hydrate growth, once the critical sized nucleus has been achieved.

1.3.1 Nucleation

Nucleation is the process where hydrate gas clusters grow and disperse in order to achieve critical size for continued growth, sometimes called catastrophic growth. The induction period is the time elapsed during the nucleation process, when hydrate nuclei are forming and dissolving in a supersaturated solution until nuclei reach the critical size. Induction time is believed to be a stochastic phenomenon and thus can not be predicted.

1.3.1.1 Factors Affecting Induction Time

Evidence suggests that nucleation is a stochastic process. Hydrate nucleation and growth may be similar to crystallization processes such as the precipitation of salt from a solution. Myers and Isaac (1907) proved metastability, which can occur through supersaturation, and hypothesized that for a concentration versus temperature profile there exists a metastable limit called the spinodal curve. Nucleation is more likely to occur when cooling past the binodal towards the spinodal curve which leads to supersaturation (Sloan, 1998a).

Induction time has been found to depend on many parameters. As stated earlier, induction time can not yet be determined theoretically since it is a stochastic process, but has been experimentally found to depend on temperature, pressure, the previous history of water (Vysniauskas and Bishnoi, 1983), stirring rate (Englezos et al., 1987; Skovborg et al., 1993), degree of supercooling (Englezos et al., 1987; Glew and Haggett, 1968b; Skovborg et al., 1993), and molecular diameter to cavity size ratio (Sloan and Fleyfel, 1991).

Vysniauskas and Bishnoi performed experiments showing that water from thawed ice or disassociated hydrates had the shortest induction times (Vysniauskas and Bishnoi, 1983). This can be explained by the fact that water retains memory and is more structured if previously in ice or hydrate form. Double distilled water was shown to have shorter induction times than that of hot tap water, suggesting that the higher the purity of water, the more structured it is.

Supersaturation is defined as the concentration of dissolved gas in solution divided by the amount of dissolved gas corresponding to three phase equilibria (hydrate-liquid-vapor). Natarajan et al. (1994) found that induction time increased with decreasing supersaturation. They suggested that high supersaturation may mask the random nature of hydrate nucleation, rendering induction time more predictable. Earlier experiments by Barlow and Hayment (Sloan, 1998a) and Parent and Bishnoi suggest that induction time is a stochastic process (Parent and Bishnoi, 1996).

Englezos et al. found that stirring rate had a significant effect on induction times. Higher stirring rates yielded shorter induction times. Other studies showing that high

turbulence gives rise to faster induction times support the observations made of the effect of stirring rate on induction time (Englezos et al., 1987).

Sloan et al. studied the ratio of guest molecule to cavity size and found that some guest molecules stabilize the hydrate structure better than others due to their size. Sloan concluded that the higher the structure stability, the shorter the induction times (Sloan, 1990).

The hydrate equilibrium point is defined as the minimum pressure at a given temperature at which hydrates can exist indefinitely. Therefore, the higher the pressure above the corresponding equilibrium pressure at a given temperature, the shorter the induction time. The same is observed as temperature is decreased below the equilibrium point. Both points mentioned above imply a greater driving force and hence a higher degree of supersaturation, which leads to shorter induction times.

1.3.1.2 Driving Force for Nucleation

The driving force for hydrate nucleation has been studied by numerous researchers, each developing their own theories. Natarajan et al. defined the driving force for nucleation to be consistent with their definition of supersaturation in the nucleation region (Natarajan et al., 1994) and can be represented by the following

$$\frac{f_i^{\exp}}{f_i^{eq}} - 1 \qquad \textbf{(1.1)}$$

where $f_i^{\exp}$ is the fugacity of the dissolved gas i at the experimental temperature (T^{exp}) and pressure (P^{exp}) conditions and f_i^{eq} is the fugacity of gas i at the three phase (vapor-liquid-hydrate) equilibrium conditions (P^{eq}, T^{exp}). P^{eq} is the three phase hydrate

equilibrium formation pressure at T^{exp}. The above expression implies that with increasing supersaturation, induction time decreases and with decreasing supersaturation induction time increases.

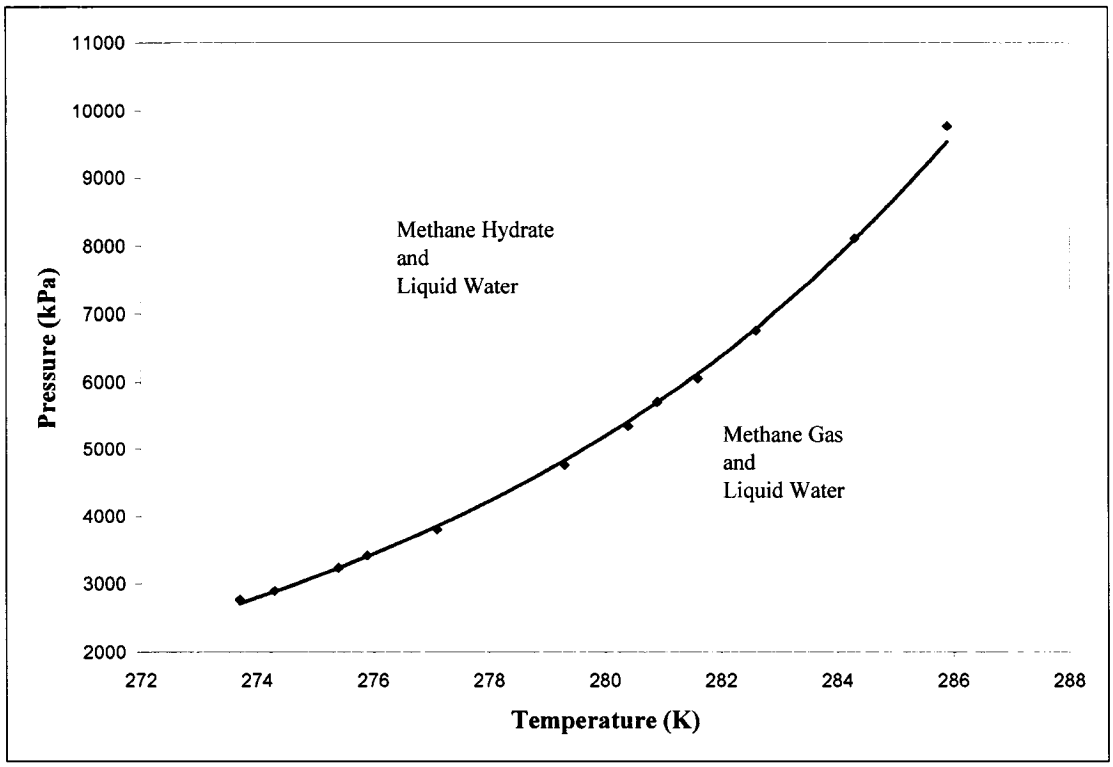

Figure 1.4: Partial phase diagram of methane (Sloan, 1998a)

Other suggested driving forces include those by Vysniauskus and Bishnoi (Vysniauskas and Bishnoi, 1983), Skovborg et al. (Skovborg et al., 1993) and Sloan and Christiansen (Sloan, 1998a). These driving forces are listed in **Table 1.1,** below.

Table 1.1: Driving forces for nucleation (reported in literature)

Investigator	Vysniauskas and Bishnoi (1983)	Skovborg et al. (1993)	Natarajan et al. (1994)	Sloan and Christiansen (1998)
Driving Force	$T^{eq} - T^{exp}$	$\mu_{wH}^{exp} - \mu_{wL}^{exp}$	$\frac{f_i^{exp}}{f_i^{eq}} - 1$	Δg^{exp}

Vysniauskas and Bishnoi suggested that at a given experimental pressure where hydrates are in three phase equilibria (vapor-hydrate-liquid), the driving force is equal to the deviation of the experimental temperature (T^{exp}) from the equilibrium temperature (T^{eq}). This difference in temperatures is also known as sub-cooling. Skovborg et al. define the driving force as the difference in chemical potential of water in the hydrate phase (μ_{wH}^{exp}) to that of water in the liquid state (μ_{wL}^{exp}) at experimental conditions. Sloan and Christiansen state that the driving force for hydrate nucleation is based on the change in molar Gibbs free energy Δg^{exp}.

1.3.2 Hydrate Crystal Growth

Hydrate nucleation is followed by crystal growth, where hydrate nuclei have achieved the critical size and continue to grow and form hydrate crystals. The growth process is affected by heat and mass transfer as well as the same factors discussed earlier regarding nucleation. Hydrate growth can be limited by factors such as diffusional barriers through crystals in gas-liquid systems. Glew and Hagget studied the kinetics of ethylene oxide hydrate formation and discovered that hydrate growth was limited by heat transfer from hydrate slurry (Glew and Haggett, 1968a, 1968b).

Pangborn and Barduhn (1970), while studying methyl bromide hydrate formation, discovered that the formation rate appeared to depend on the kinetics of the interfacial reaction to form crystals. Graauw and Rutton, while using chlorine and propane as hydrate formers, showed that mass transfer at the hydrate-forming substance-water interface can be a rate-determining factor in hydrate formation. It was also found that the

hydrate formation reaction at the surface can be a rate-determining step (De Graauw and Rutten, 1970).

A comprehensive model incorporating crystallization theory was developed by Englezos et al. at the University of Calgary (Englezos et al., 1987). The model is a mechanistic one with one adjustable parameter per hydrate former. It is assumed that the nucleus forms instantaneously by primary homogeneous nucleation. It should be pointed out that homogenous nucleation is impossible since impurities can never be fully removed from the liquid water. The driving force for hydrate crystallization at the experimental temperature is the difference in the fugacity of the dissolved gas, f, and the three phase equilibrium fugacity, f_{eq}. The driving force

$$\Delta f = f - f_{eq} \tag{1.2}$$

is determined by the deviation from the three phase equilibrium vapor-liquid-hydrate conditions.

Hydrate kinetics is commonly monitored using a method based on measuring the amount of hydrate forming gas consumed as a function of time (Englezos et al., 1987). Another method based on crystal thickness measurements coupled with morphology was used by Makogon (Makogon and Editor, 1997). Raman spectroscopy has also been used to provide kinetic spectra describing the transition from dissolved methane to methane hydrate (Sloan, 1998b). X-ray diffraction is yet another method that has been applied to carbon dioxide hydrates (Takeya, 1999).

Light scattering techniques have been examined by Nerheim et al. (Nerheim et al., 1992), Monfort and Nzihou (Monfort and Nzihou, 1993), Bylov and Rasmussen (Bylov and Rasmussen, 1996), and Parent (Parent, 1993) in order to study hydrate growth

kinetics. Results have been inconsistent due to the extremely small size of nuclei, which makes measurements of the rate of crystal growth using light scattering techniques very difficult to obtain. Laser light scattering experiments were performed by Servio et al. (Servio, 2002) on ethane hydrate in the absence and presence of monodispersed latex particles. Results were inconclusive due to problems such as unknown size, shape, number of particles and effect of agitation, among others.

1.3.3 Hydrate Decomposition

Hydrate decomposition may be viewed as a two step process; the destruction of the clathrate host lattice at the particle surface followed by desorption of the guest molecule from the surface. Thermal decomposition of hydrates is an important study in the field of heat transfer. In the case of propane hydrates, decomposition has been linked to the rate of heat transfer which is correlated with an expression that includes the temperature driving force (Kamath et al., 1984). Kim et al. suggested the driving force for methane hydrate decomposition to be proportional to the difference between the fugacity of methane at the hydrate-vapor-liquid equilibrium conditions and the fugacity of methane in the bulk gas phase (Kim et al., 1987).

1.4 Inhibition of Gas Hydrates

Gas hydrates are problematic in the oil and gas industry because they have been found to block pipelines, causing severe damage to equipment such as pumps and

compressors. The prevention of gas hydrate formation is the motivation for research in hydrate inhibition.

All three naturally occurring hydrate structures (structure I, structure II and structure H) consist of approximately 85% water on a molecular basis and many of the mechanical properties of hydrate are similar to those of structure Ih ice. Due to these similarities in structure, studies of growth inhibition performed on ice are often related to the inhibition of hydrate growth.

There are three types of inhibitors that affect hydrate nucleation and growth, thermodynamic inhibitors, anti-agglomerants and kinetic inhibitors.

1.4.1 Thermodynamic Inhibition

Thermodynamic inhibitors shift hydrate equilibrium conditions such that the operational conditions are moved outside the hydrate forming region; in other words, outside the temperature and pressure region at which hydrates are thermodynamically stable. There are four ways of achieving this: increasing temperature, decreasing pressure, removing one of the hydrate-forming components (either guest substance or water) or injecting chemicals that alter the equilibrium conditions. Methanol is an example of a thermodynamic inhibitor that alters the equilibrium conditions of hydrate formation.

1.4.2 Anti-agglomerants

Another method used to prevent hydrate plugs is by making use of anti-agglomerants, which suspend hydrate crystals in condensate. This occurs because ends of anti-agglomerant particles have qualities attractive to both hydrates and oil. This causes the dispersion of hydrates as small masses in oil, preventing the hydrate accumulation under proper water/oil ratios (Huo et al., 2001). Some anti-agglomerants also interfere with hydrate kinetics, making for a particularly effective hydrate inhibitor (Davies et al., 2002).

1.4.3 Kinetic Inhibition

Kinetic inhibitors are polymer based compounds that interfere with hydrate nucleation and/or growth. The purpose of kinetic inhibition is to prolong the period prior to catastrophic growth beyond the fluid residence time in a pipeline. One advantage of kinetic inhibitors is that dosages required in order to be effective are lower than those required for thermodynamic inhibitors. A further advantage is that they often act as anti-agglomerants as well.

1.4.3.1 Lactam Ring Polymers

Lactam ring polymers have been found to be effective kinetic inhibitors. Lactam rings are characterized by an amide group attached to a polymer backbone. Chemical structures of some of the most effective lactam ring polymer inhibitors are given in **Figure 1.5**.

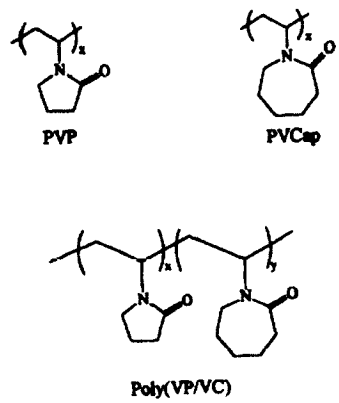

Figure 1.5: Chemical structures of some effective kinetic inhibitors (Lederhos et al., 1996)

Polyvinylpyrrolidone (PVP) consists of five-member lactam rings attached to a carbon backbone. Molecular weights for these polymers typically range from 10,000 g/mol to 350,000 g/mol. A similar kinetic inhibitor, poly(N-vinylcaprolactam), or PVCap, belongs to the same family of lactam ring polymers as PVP and is characterized by a seven-member lactam ring protruding from a polymeric backbone. Poly(VP/VC) is a copolymer of PVP and PVCap and is thus characterized by five-member and seven-member lactam rings.

It has been suggested by Lederhos et al. that during hydrate growth, lactam rings adsorb onto the hydrate crystal through hydrogen bonding by the amide group, sterically

blocking hydrate growth. Furthermore, they suggested that a polymer network extends between small stabilized hydrate particles, possibly providing an inhibiting structure to the surrounding water while blocking the most active growth sites of hydrate crystals. More studies are being performed in order to analyze this hypothesis more thoroughly (Lederhos et al., 1996).

1.4.3.2 Antifreeze Proteins

Antifreeze proteins (AFPs) are another example of kinetic inhibitors. During ice formation, most proteins will be excluded and thus pushed ahead of the expanding ice front. Raymond and DeVries claim that AFPs are different in that they adsorb to the ice front, restricting growth to regions between the adsorbed protein molecules (Raymond and DeVries, 1977). These regions thus grow with local curvature, making thermodynamically unfavorable conditions for continued ice growth (Wilson, 1993). This is referred to as the adsorption-inhibition hypothesis. The above mechanism depresses the freezing point of water, a phenomenon called thermal hysteresis.

Antifreeze glycoproteins were discovered by DeVries et al. in 1969 (DeVries and Wohlschlag, 1969). Several other AFP types have been characterized since in distinct groups of teleosts in both the northern and southern hemispheres. The various AFP types are very different in their primary sequences and 3D structure, yet they all bind to ice and depress the non-equilibrium freezing point below the melting point. The need for AFPs in fish is recent, which explains the structural diversity in fish AFPs. However, there is considerable diversity in insect and plant AFPs, indicating that climate change may have affected insects after evolutionary divergence. Ice can present many different surfaces with various geometric arrangements of oxygen atoms and any protein with an affinity

for one of these planes may serve as an antifreeze prototype on which natural selection can act to improve binding efficiency (Davies et al., 2002).

The antifreeze protein used as a kinetic inhibitor for experiments was Type I antifreeze protein, a rod-like alpha-helix obtained from the winter flounder (*pseudopleuronectes americanus*) (**Figure 1.6**).

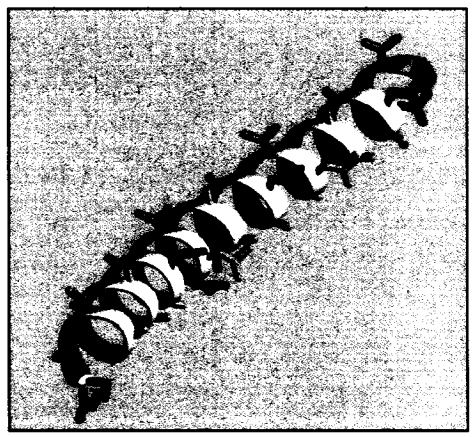

Figure 1.6: Type-I antifreeze protein (http://pout.cwru.edu/~frank/afp1/)

1.5 Gas Hydrate Morphology

Crystal morphology studies are important in terms of providing valuable insight into the mechanistic aspects of hydrate nucleation, growth and decomposition. The first hydrate crystal morphological studies were performed by Makogon using a rectangular, windowed container without mixing for experimentation (Makogon, 1994). He obtained hydrate crystals using different components of natural gases and reported various geometries such as thread-like, spherulitic, film-like, dendritic, and viscera-like, among others, which are accredited to many factors including variation in hydrate forming gas, degree of supercooling, experimental pressure and location of hydrate nucleation.

Studies by Maini and Bishnoi and Topham reported observations of clathrate hydrate formation on methane bubbles or natural gas released in a down flow of seawater in a simulated deep sea environment (Maini and Bishnoi, 1981; Topham, 1984). Observations suggested that hydrate formation occurred on the bubble and continued to grow until the bubble was enclosed by a hydrate layer. The bubble surface became more rigid in shape while maintaining flexibility. Furthermore, flakes of hydrate from the rear of the bubble broke free, separating from the bubble.

Aya et al. and Shindo et al. placed carbon dioxide droplets on a solid plate and a wire grid respectively, immersed in quiescent water or seawater not saturated with carbon dioxide (Aya et al., 1993; Shindo et al., 1993). The experiments were performed at pressures corresponding to those at a depth of 3 km in seawater (30 MPa). Both observed immediate formation of a thin, smooth, semi-transparent hydrate film on the surface of each droplet. As well, both researchers concluded that hydrate coated droplets decreased in diameter over time at rates appreciably lower than those for uncoated droplets.

In 1994, Nojima and Mori studied hydrate forming fluorocarbon systems (CFC-11 and HFC-141b). One bubble of fluorocarbon was held stationary in a down flow of water. Hydrate first appeared on the surface of each bubble in the form of tiny particles, which were swept to the back of the bubble and accumulated until a hydrate layer surrounded the entire bubble (Nojima, 1994). The observations were consistent with previously reported morphological observations (Maini and Bishnoi, 1981; Topham, 1984). Nojima and Mori (1994) also noted that with time, the fragile bubble crumbled due to hydrodynamic shear imposed by the down flow of water. Nojima and Mori also observed the shrinkage of bubbles occurring more rapidly on bubbles with hydrate than

on hydrate free bubbles, concluding that the hydrate covering is porous and does not impede rate of dissolution of fluorocarbon in the water. This observation is in disagreement with work by Shindo et al., who observed more rapid shrinkage in hydrate free carbon dioxide droplets (Shindo et al., 1993).

Morphological studies were carried out by Sugaya and Mori on the boundary of fluorocarbons (HFC-134a, CH_3CH_2F) in the vapor or liquid state and water (Sugaya and Mori, 1996). Experiments were performed on fluorocarbon droplets of 4.5 - 6.5 mm in diameter as well as on planar interfaces between fluorocarbon and water. Observations indicated that degree of supersaturation of the water phase with the fluorocarbon strongly influences the surface morphology of the hydrate layer. The mechanical structure of the hydrate layer was found to be independent of the state of the fluorocarbon (vapor or liquid) but was strongly dependent on hydrodynamic conditions near the interface. Observations of the rate of shrinkage on fluorocarbon droplets were in agreement with Shindo et al. (1993). They concluded that the hydrate layer formed on the surface of a fluorocarbon droplet held stationary is not as porous as the coagulation of hydrate particles observed on the surface of buoying fluorocarbon-vapor bubbles (Nojima and Mori, 1994).

Sugaya and Mori conducted experiments on fluorocarbon droplets in the presence of saturated and not saturated water. Findings indicate that in both cases the hydrate phase grows quickly on the surface of each droplet until extending over the entire surface. The surface morphology established in the early process is maintained if the surrounding water is saturated. If the surrounding water is not saturated, the initial morphology faded quickly and the surface of the hydrate shell became a smooth and of

fine texture. After extended periods of time, the hydrate-coated droplet decreased in diameter in the unsaturated water while maintaining a smooth shell surface throughout. It was hypothesized that the hydrate shell maintained a smooth surface while shrinking due to a continuous renewal and decomposition of hydrate on the shell (Sugaya and Mori, 1996).

Mori and coworkers (Ohmura et al., 1999) continued to study the growth and dissociation of hydrate crystals in liquid water in contact with a hydrophobic hydrate forming liquid. The liquid-hydrochlorofluorocarbon used was R-141b, known to form structure II hydrate. Experiments were carried out with pure water or presaturated water in contact with R-141b at the approximate three-phase equilibrium temperature and various degrees of sub-cooling. Observations showed that presaturated water at high sub-cooling (~ 6.5 K) exhibited two stages of hydrate crystal growth, which varied not only in crystal morphology but also in length of time. The first stage was characterized by lateral crystal growth of a thin, fine-grained polycrystalline layer along the R-141b surface and was observed for several tens of seconds. The later stage began with a delay of approximately 10 minutes and continued for a few tens of hours, exhibiting radial growth of plate-like crystals standing upright on the outer surface of the drop-enclosing hydrate shell formed in the first stage. An increase in temperature below the three phase temperature produced the dissolution of the plate-like crystal, leaving the hydrate shell seemingly unchanged. The later stage was not observed in the presence of pure water and/or with small sub-cooling (~ 2 K).

Kato et al. (Kato, 2000) performed experiments investigating the droplet formation behavior of a hydrophobic hydrate forming liquid, HCFC-141b (CH_3CCl_2F), at

a single nozzle in a stream of water under hydrate forming thermodynamic conditions. Two discrete hydrate crusts were observed growing along the liquid-liquid interface. One formed a frontal cap and the other formed a cylindrical root on each growing droplet before detachment from the nozzle. Over the course of successive growth and detachment of droplets, a crust remained at the tip of the nozzle after detachment of the droplet, growing into a bell-shaped or nearly cylindrical funnel composed of hydrate deposits. The size of each droplet depends on the instantaneous diameter of the hydrate funnel tip rather than the diameter of the nozzle itself. The size of each droplet successively released into the water stream varied with alternation of growth and breaking of the hydrate funnels, which in turn significantly depends on system temperature, nozzle diameter, and velocity of the droplet forming liquid through the nozzle.

Servio and Englezos formed methane and carbon dioxide hydrates from water droplets at 274.6 K and 2150 kPa, 1000 kPa above the corresponding hydrate equilibrium pressure (Servio and Englezos, 2003). At the higher pressure the hydrated droplets were jagged and displayed fine needle-like crystals protruding from the droplet surface. At lower pressures, or a lower driving force, the jaggedness was not observed. The texture of the droplet was smooth and shiny. The difference observed in surface roughness at high and low driving force is hypothesized to depend on the density of the hydrate nuclei formed which depends on the magnitude of the driving force. Under a high driving force, nucleation will occur on the surface at a larger number of sites relative to a low driving force. Rate of nucleation has been found to increase with degree of supersaturation (Kubota et al., 1997), which is in turn proportional to the driving force. Under a high

driving force, fast nucleation kinetics will cause more random crystal growth and hence a rough surface.

Xie et al. studied gas hydrate growth morphology of HCFCl141b outside of a horizontal heat transfer tube. Growth was observed with and without sodium dodecyl sulfate (SDS). It was found that heat of formation of gas hydrate was adsorbed more quickly in a system with SDS rather than a system without, leading to a faster rate of hydrate growth (Xie et al., 2005).

1.6 Research Objectives

Preventing hydrate formation is important in the oil and gas industry, creating a demand for hydrate inhibition research. This thesis focuses on studying the morphology of structure I methane hydrate under the effect of kinetic inhibitors such as a lactam ring copolymer and antifreeze protein, which will be discussed in further detail in the following section. It will include observations made during nucleation, growth and decomposition of methane hydrate, all of which are fundamental in terms of understanding the mechanistic aspects of hydrate formation.

The research objectives of this thesis are as follows:

- To design a high pressure crystallizer capable of withstanding pressures of up to 20,000 kPa.
- To build the experimental apparatus and set-up necessary to perform morphological studies on methane hydrate.
- To study the morphology of structure I methane hydrate on water droplets in the presence of kinetic inhibitors during nucleation, growth and decomposition with a high speed camera.

2 EXPERIMENTAL APPARATUS AND PROCEDURE

2.1 Crystal Morphology

A description of the experimental apparatus for morphology studies of structure I methane hydrate formed from water droplets in the presence of kinetic inhibitors is given in the following section. Morphology studies were performed with the use of a high speed camera capable of taking up to 636 frames per second (exposure time of 1.57 ms). An objective lens with a magnification of 20X was used for experimentation.

2.1.1 Apparatus (Structure I Morphology)

The main component of the experimental apparatus consisted of a high pressure crystallizer able to withstand pressures up to 20,000 kPa with an internal volume of approximately 77 cc. The crystallizer was constructed of a sapphire tube 6 inches in length by Insaco Inc. held in place by two stainless steel supports and three titanium rods as shown in **Figure 2.1**. The inner diameter of the tube was 1 inch and the outer diameter was 1.5 inches, yielding a tube wall thickness of 0.25 inches. Assembled, the exposed length of the sapphire tube was 4 inches.

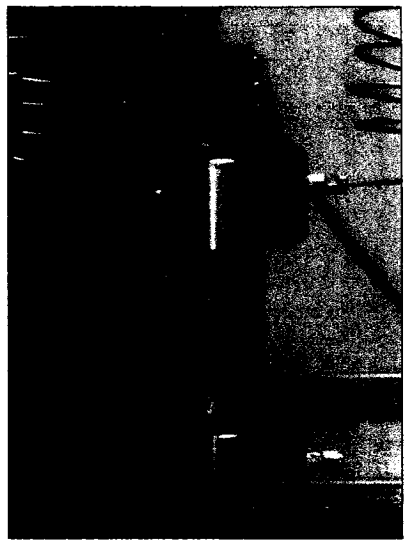

Figure 2.1: Picture of high pressure crystallizer

All components of the reactor were cleaned with soap and water, rinsed with distilled water and allowed to dry completely before assembly. The surface of a stainless steel rod, 0.5 inches in diameter and 1.5 inches in height, was coated with polytetrafluoroethylene tape (Teflon tape) and placed inside the reactor. A 10 μL Hamilton syringe was used to make droplets. It was found that a 5 μL volume yielded droplets 2.5 mm in diameter, measured using calipers. Three droplets 2.5 mm in diameter were placed on the Teflon coated bar as shown in **Figure 2.2**. The droplets were either pure water or water in the presence of kinetic inhibitors depending on the experiments being performed.

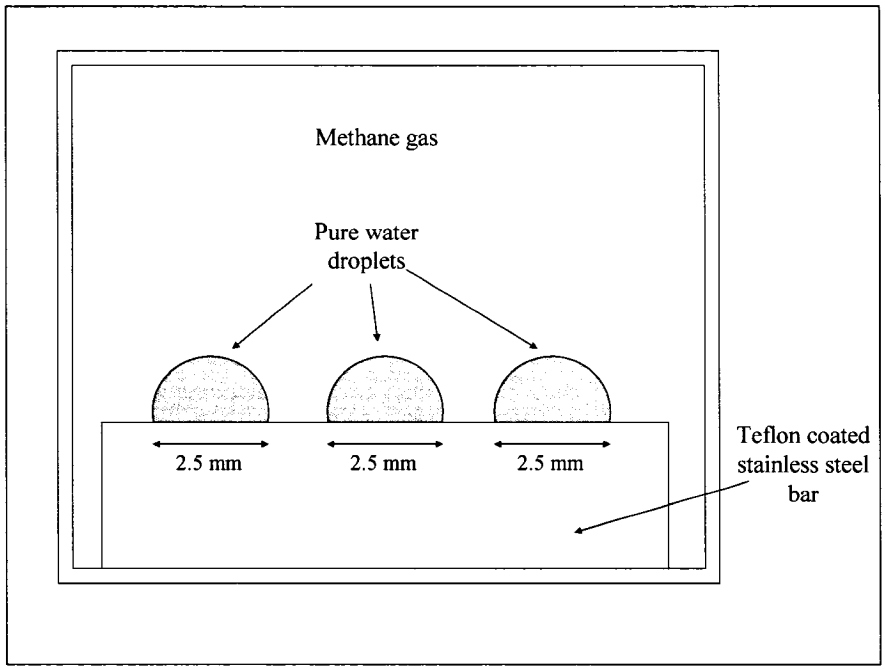

Figure 2.2: Schematic of inside of reactor (not to scale)

The reactor was placed in a bath with a 50-50 volume % mixture of ethylene glycol and water which was maintained at a constant temperature by a Thermoelectron RTE-17 refrigeration unit. The refrigeration unit also ran a 50-50 volume % water and ethylene glycol mixture through a copper coil immersed in the bath. The cooling medium was circulated throughout the bath with the aid of a motorized impeller in order to maintain a constant temperature. The temperature of the gas phase in the reactor was monitored with a type T RTD with an accuracy of +/- 0.1K. The pressure in the crystallizer was measured with a Rosemount Smart pressure transducer (3051CD, Norpac Controls) having a range of 0-13,790 kPa and an accuracy of 0.04 percent. The pressure transducer and RTD were both connected to a data acquisition system in order to monitor the pressure and temperature in the reactor. The stainless steel bath was equipped with clear polymethylmethacrylate (PMMA) viewing windows. Two Schott KL 2500 fiber

optic light pipes provided illumination for the high speed camera. **Figure 2.3** below shows a simplified schematic of the laboratory set-up.

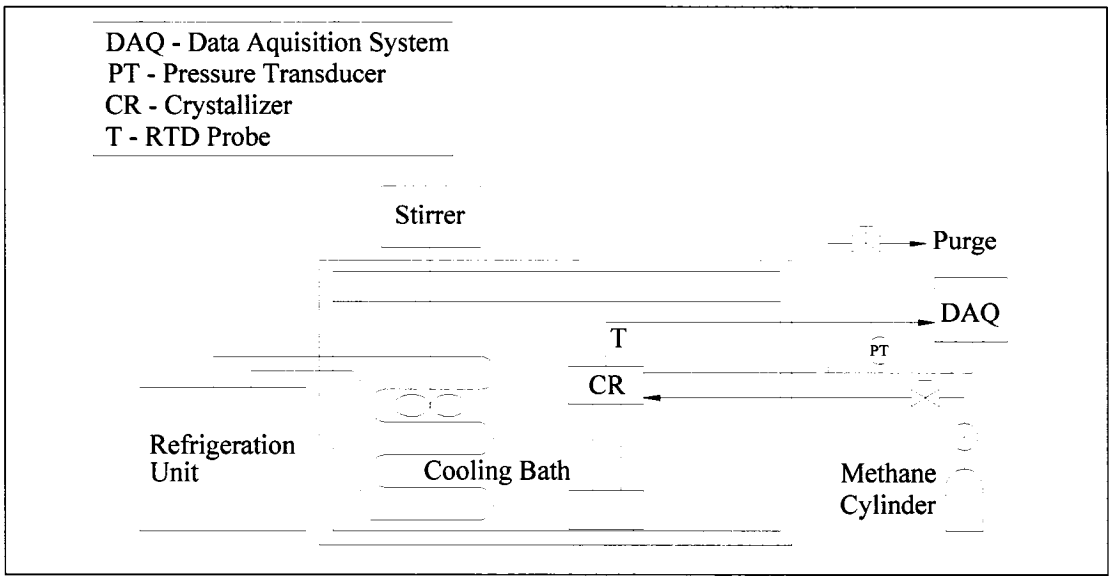

Figure 2.3: Simplified schematic of laboratory set-up (not to scale)

2.1.2 Crystal Morphology Procedure for Structure I Hydrate

The inside of the crystallizer as well as the stainless steel cylinder and Teflon on which the droplets were placed were cleaned and all moisture was removed. The apparatus was tested for leaks by pressurizing the system up to 5000 kPa and verifying the presence of either bubbles in the cooling bath or by using Snoop® on fittings not submerged in the bath. A constant pressure drop over time indicates the presence of one or more leaks in the system.

Initial experiments were performed with distilled and de-ionized water droplets. It was found that a 5 μL volume of water resulted in a droplet 2.5 mm in diameter. Three droplets were placed on the Teflon coated cylinder in order to prevent the droplets from wetting the surface with the use of a Hamilton 10 μL syringe. Care was taken to avoid

contact between the tip of the syringe and the Teflon tape since this could possibly puncture the Teflon. The reactor was closed and flashed three times with the experimental gas at a pressure of 1000 kPa to remove any possible residual gas in the reactor. The experimental gas, ultra high purity CH_4 (UHP CH_4), was then fed into the reactor from a cylinder. The temperature in the reactor was maintained constant at 275.2 K. The equilibrium pressure for CH_4 at this temperature is 3020 kPa. Experiments were performed on pure water at pressures of 5000 and 7200 kPa.

In subsequent experiments, inhibitors were introduced into the system (**Figure 2.4**). One droplet of pure water was placed on the Teflon coated bar. A second droplet containing 0.01 mM of a 50/50 molar ratio of PVP and PVPCap (poly(VP/VC)) was placed next to the first droplet. Finally, a third droplet containing 0.01 mM of antifreeze protein (AFP) was placed next to the second. Experiments were performed at pressures of 5000 kPa, 6500 kPa, 7200 kPa and 10,000 kPa.

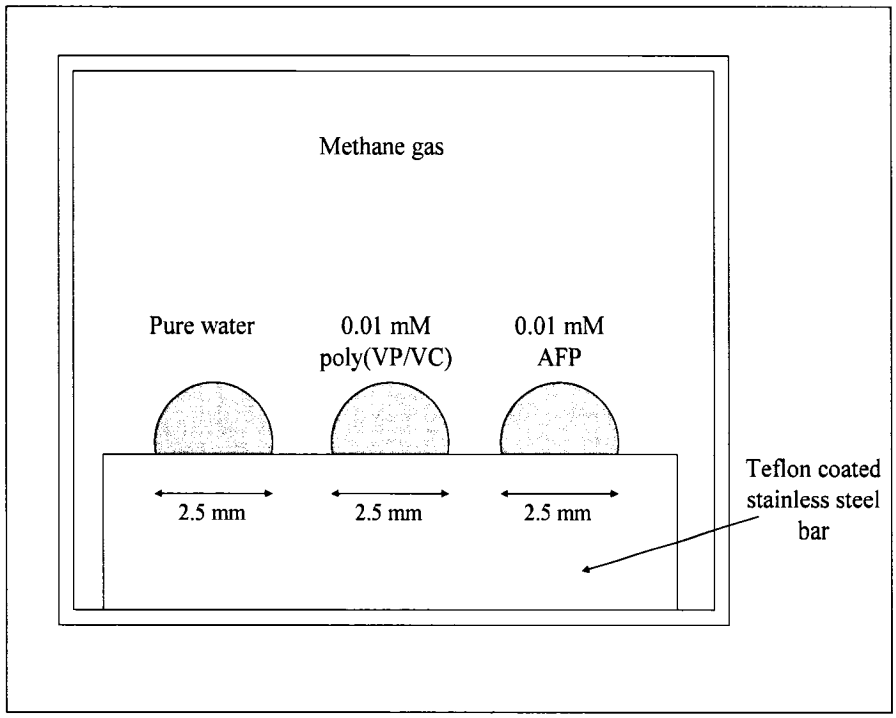

Figure 2.4: Simplified schematic of droplets inside crystallizer (not to scale)

Many different lighting positions were tested in order to find the best viewing of the droplets. A Schott KL 2500 fiber optic light pipe was used. It was found that lighting from the back of the cooling bath did not give off enough illumination to view surface properties of the droplets. After obtaining a second identical light pipe and trying several combinations of positions, it was found that with one light pipe illuminating from either side of the reactor provided ideal viewing of the droplets.

3 A MORPHOLOGY STUDY OF STRUCTURE I METHANE HYDRATE

Macroscopic crystal morphology studies were performed on structure I methane hydrate formed on pure water droplets as well as water droplets in the presence of kinetic inhibitors. In this study, two kinetic inhibitors were investigated. The first was a lactam ring copolymer, poly(VP/VC), a mixture of polyvinylpyrrolidone (PVP) and polyvinylcaprolactam (PVCap) in a 50/50 molar ratio. The second was antifreeze protein obtained from the winter flounder (*pseudopleuronectes americanus*). Three 2.5 mm droplets were placed side by side on a Teflon-coated stainless steel bar inside the crystallizer at a temperature of 275.2 K and various experimental temperatures as depicted in Section 2.1.1. Experiment results are discussed in the following sections.

3.1 Effect of Pressure on Induction Times of Pure Water Droplets

Experiments were performed on three distilled and de-ionized water droplets 2.5 mm in diameter. The inside of the crystallizer was cooled to a temperature of 275.2 K and pressurized at two different experimental pressures, 7200 and 5000 kPa, in order to observe the effect of driving force on induction times. The experimental pressures correspond to 4180 kPa and 1980 kPa, respectively, above the three-phase hydrate equilibrium pressure of 3020 kPa (Sloan, 1998a) at the experimental temperature. Results are summarized in **Table 3.1**.

Table 3.1: Experimental conditions and induction times of three pure water droplets 2.5 mm in diameter

Exp	Memory (hrs)	T (K)	P (kPa)	Induction time droplet 1 (min)	Induction time droplet 2 (min)	Induction time droplet 3 (min)
1	n/a	275.2	7200	137	138	140
2	1	275.2	7200	3	2	3
3	1	275.2	5000	*	*	*

n/a indicates fresh droplets
memory refers to the time between hydrate decomposition and reformation
* indicates no nucleation after 4 hours

In experiment 1, at high pressure and with no memory, the first droplet (left) formed hydrate within 137 minutes. The second (middle) formed 1 minute later followed by the third (right) 3 minutes after the first. A communication effect may be responsible for all three droplets forming hydrate within 3 minutes of each other. It is hypothesized that the communication effect can be attributed to physical contact between the droplets due to dendritic growth extending from the surface of a hydrate covered droplet to a water droplet that has yet to form hydrate. The dendrite touches another supersaturated water droplet and initiates nucleation of a hydrate crystal on that droplet. These dendrites may be too small to capture under the current magnification but in some cases dendrites were observed to bridge between two droplets. Another possibility is that one or more hydrate seeds could be transported through the gas phase to land on another droplet, inducing nucleation.

When decomposed, left for one hour, and reformed (experiment 2), all droplets formed hydrate within 1 minute of each other. This may have been caused by a memory effect. On the other hand, one hour might not have been sufficient time for complete decomposition of the hydrate. Seeds may have remained on the droplet(s), causing shorter induction times.

In experiment 3, at a low pressure and with a memory of 1 hour, hydrate did not form within 4 hours and the experiment was terminated. It was found that pressures in excess of 5000 kPa were required in order for the hydrate crystals to form, even with memory effects, within a reasonable amount of time. Additional longer-lasting experiments would need to be performed in order to collect conclusive data at such a driving force.

To summarize, it was found that with no previous memory and under identical temperature and pressure conditions, nucleation occurred on three pure water droplets within 3 minutes of each other. It is hypothesized that a communication effect is responsible for this phenomena. During reformation experiments, at pressures above 5000 kPa, simultaneous nucleation occurred. This can be explained by a communication effect, a memory effect or a combination of the two.

3.2 Effect of Pressure on Induction Times of Water Droplets in the Presence of Kinetic Inhibitors

The effect of two kinetic inhibitors on induction times was studied in this set of experiments and the results summarized in **Table 3.2**. The first was a lactam ring copolymer, a mixture of PVP and PVPCap in a 1:1 molar ratio dissolved in water, or poly(VP/VC). The copolymer was obtained from BASF and had an average molecular weight of 7 kDa. The other inhibitor used was purified type I antifreeze protein obtained from the winter flounder (*pseudopleuronectes americanus*) with an average molecular weight of 4 kDa. It was purchased from A/F Protein Canada. Each inhibitor was dissolved in water to yield a concentration of 0.01 mM. Two water droplets 2.5 mm in

diameter, each containing kinetic inhibitor, were placed in the reactor on a Teflon-coated stainless steel surface alongside a third droplet of pure water.

Table 3.2: Experimental conditions and induction times of 2.5 mm droplets in the presence of kinetic inhibitors.

Exp	Memory (hrs)	T (K)	P (kPa)	Induction time water droplet (min)	Induction time poly(VP/VC) droplet (min)	Induction time AFP droplet (min)
4a	n/a	275.2	10000	259	290	260
4b	1	275.2	10000	2	2	3
4c	1	275.2	7200	2	3	3
4d	1	275.2	5000	11	*	*
5	n/a	275.2	7200	*	*	*
6a	n/a	275.2	7200	413	584	508
6b	1	275.2	7200	9	5	3
6c	1	275.2	7200	2	1	1
6d	1	275.2	7200	62	2	2
6e	1	275.2	6500	4	3	49
6f	1	275.2	6500	4	6	6
6g	1	275.2	6500	*	*	*
7	n/a	275.2	7200	*	*	*
8	n/a	275.2	7200	*	*	*
9a	4	275.2	7200	19	15	12
9b	1	275.2	7200	1	2	4
9c	1	275.2	7200	4	3	4
9d	1	275.2	6500	2	3	2
9e	1	275.2	6500	*	4	3

n/a indicates fresh droplets
memory refers to the time between hydrate decomposition and reformation
* indicates no nucleation after 24 hours

Induction times were measured on droplets without memory at pressures of 10,000 and 7200 kPa. At 10,000 kPa (experiment 4a), the induction time of the water droplet was 259 minutes. The AFP droplet formed 1 minute later. This small difference in induction times may be the result of a communication effect as described in Section 3.1. The poly(VP/VC) droplet nucleated 31 minutes after the first droplet to form hydrate.

At a pressure of 7200 kPa and without memory (experiment 6a), induction times were higher, as anticipated, due to a decrease in the driving force. The induction times of the water droplet, poly(VP/VC) droplet and AFP droplet were 413, 508 and 584 minutes, respectively. However, in all other experiments under similar experimental conditions (experiments 8, 16 and 17) no hydrate formation was observed in 24 hours and experiments were terminated. This can be justified by the fact that nucleation is a stochastic process and induction times are hard to predict. Longer lasting experiments would need to be performed in order to observe a trend. It can be concluded nonetheless that with no memory effect, the water droplet tends to nucleate before the droplets with inhibitors. It has been proposed by previous researchers that lactam ring polymers and antifreeze proteins bind to crystals, preventing growth in the respective plane (Chapsky and Rubinsky, 1997; Davies et al., 2002; Du et al., 2003; Larsen et al., 1996; Nguyen et al., 2004; Strom et al., 2004). The polymer chains and antifreeze protein molecules each may affect nucleation by interfering with the formation and dispersion of unstable nuclei, resulting in longer induction times.

Experiments were performed on droplets with memory at 10,000 kPa, 7200 kPa, 6500 kPa and 5000 kPa. Only one experiment was done at 10,000 kPa (experiment 4b) and all droplets formed hydrate within 1 minute of each other. It should be noted that in nine of fourteen experiments on droplets with memory, a droplet with inhibitor nucleated prior to the water droplet. Since these are reformation experiments the explanation for this phenomenon could be that the kinetic inhibitors preserve hydrate crystals by slowing down hydrate decomposition, therefore, hydrate seeds may still be present when the pressure is increased back above the three-phase pressure. Crystals then begin to grow

on the droplets containing inhibitors while the pure water droplet has to nucleate its own seeds once again. A communication effect may be responsible for immediate nucleation of one droplet after another.

At 7200 kPa, droplets formed hydrate within 7 minutes of each other in five of the seven experiments (experiments 4c, 6b, 6c, 9a, 9b and 9c). In experiment 6d, there was a 60 minute difference between the first and last droplet to form hydrate. Nucleation occurred on the poly(VP/VC) droplet or AFP droplet before the water droplet in five of seven experiments. Since the water droplet consistently decomposed before the other two droplets, more time was allowed for full decomposition and for all hydrate seeds to die. The droplets with inhibitors decomposed slower than the water droplet and may still have had seeds on the droplet surface, causing shorter induction times in subsequent reformation experiments.

At a lower pressure of 6500 kPa, five experiments were performed. There were larger differences in induction times, possibly due to the fact that under lower driving forces, the nucleation process behaves more stochastically. In experiments 6f and 9d, all droplets formed hydrate within 2 minutes of each other. In experiment 6e, the poly(VP/VC) and water droplet formed hydrate within a minute of each other but the AFP droplet did not form until 46 minutes after the first. It is interesting to note also that in experiment 9e, the poly(VP/VC) droplet and AFP droplet formed within a minute of each other and yet the water droplet did not form in less than 24 hours and the experiment was terminated. In experiment 6g, no nucleation occurred within 24 hours on any of the droplets. The variation in induction times indicates that nucleation truly is a stochastic process if there is no influence by a communication effect or the presence of seeds.

One experiment was performed at 5000 kPa and no nucleation occurred within 24 hours. It was deemed that at 5000 kPa the nucleation times might be too large (in the order of days) and all further experiments under these conditions were abandoned.

Overall, the higher the driving force, the shorter the induction times when forming crystals on droplets with no previous history of hydrate formation. This can be seen by comparing experiments 4a and 6a. The higher pressure experiment, 4a, led to induction times significantly smaller, almost half, of experiment 6a. When hydrates are formed on crystals with previous history, there is no apparent correlation between pressure and nucleation and induction times observed are very small. This is probably due to incomplete decomposition of the hydrate crystal in the 1 hour time allotted for decomposition. Hence, when thermodynamic conditions favor the birth of the crystal phase, the nucleation step is bypassed and the nuclei still present begin to grow almost immediately.

3.3 Crystal Morphology during Hydrate Nucleation and Growth

Droplets were observed with the use of a high speed camera as described in Section 2.1 with and without kinetic inhibitors. It was noticed in all cases that nucleation occurred at a certain point on the surface of the droplet and not in several areas. Once nucleated, hydrate crystal growth proceeded radially until the entire surface of the droplet was covered in a thin hydrate skin. An example of the progression of this surface coverage from experiment 6d is shown in **Figure 3.1** on a poly(VP/VC) droplet. The arrow points to the area of nucleation. Hydrate skin thickness could not be accurately measured and observations were purely visual.

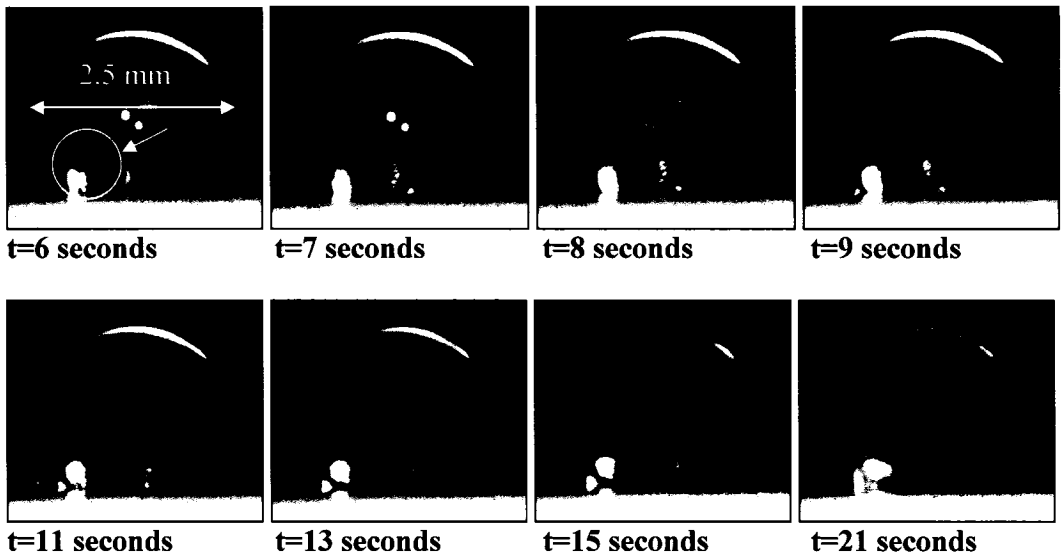

Figure 3.1: Nucleation and progression of radial growth (experiment 6d)

A progression of nucleation and growth on all three droplets in experiment 6c is shown in **Figure 3.2** at various times. The experiment was performed at a pressure of 7200 kPa and a temperature of 275.2 K. The droplet in the middle, the poly(VP/VC) droplet, nucleated first, followed by nucleation of the AFP droplet. The pure water droplet nucleated last.

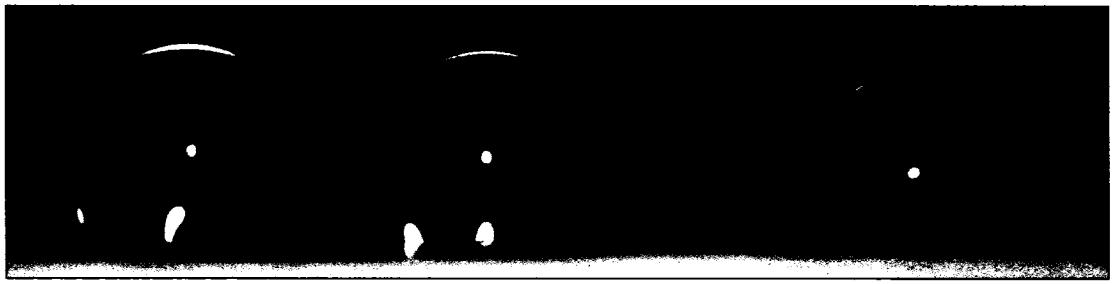

Figure 3.2a: t=0. Left: pure water. Middle: poly(VP/VC) 0.01 mM. Right: AFP 0.01 mM.

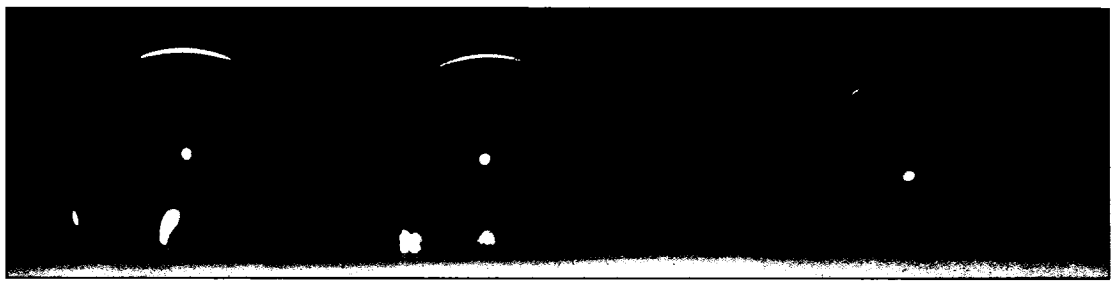

Figure 3.2b: t=10 seconds. Hydrate nucleation on poly(VP/VC) droplet.

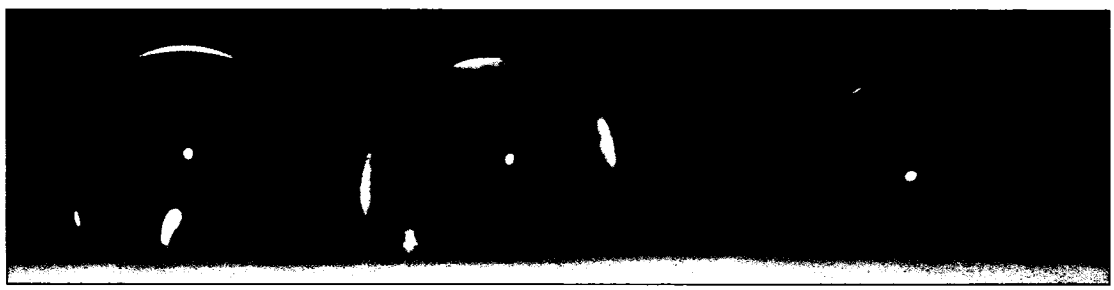

Figure 3.2c: t=15 seconds. Hydrate crystal growth on poly(VP/VC) droplet.

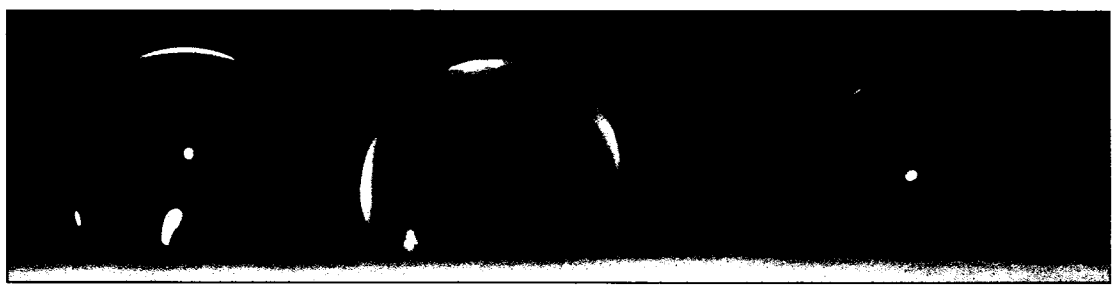

Figure 3.2d: t=20 seconds. Full surface coverage of poly(VP/VC) droplet.

Figure 3.2e: t=50 seconds. Hydrate nucleation on AFP droplet.

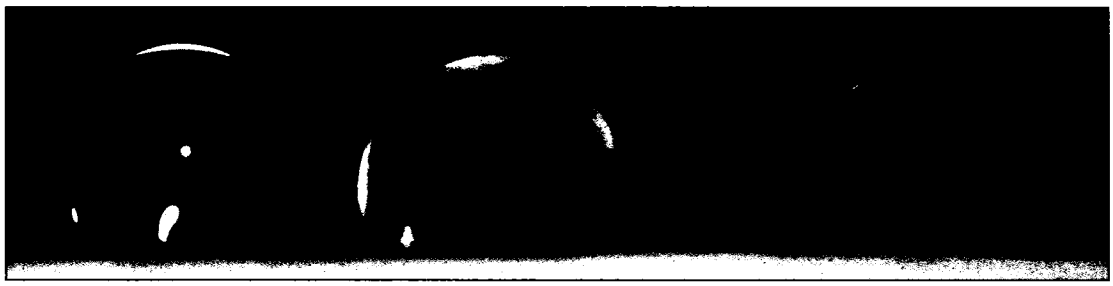

Figure 3.2f: t=55 seconds. Hydrate crystal growth on AFP droplet.

Figure 3.2g: t=60 seconds.

Figure 3.2h: t=75 seconds. Full surface coverage of AFP droplet.

Figure 3.2i: t=90 seconds. Hydrate nucleation on pure water droplet.

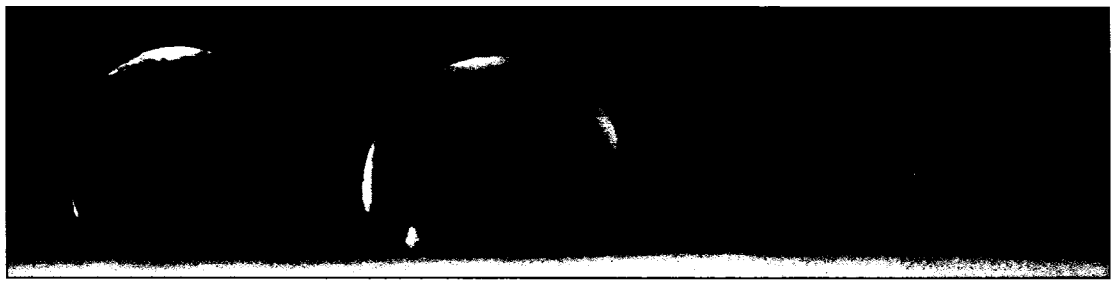

Figure 3.2j: t=95 seconds. Hydrate crystal growth on pure water droplet.

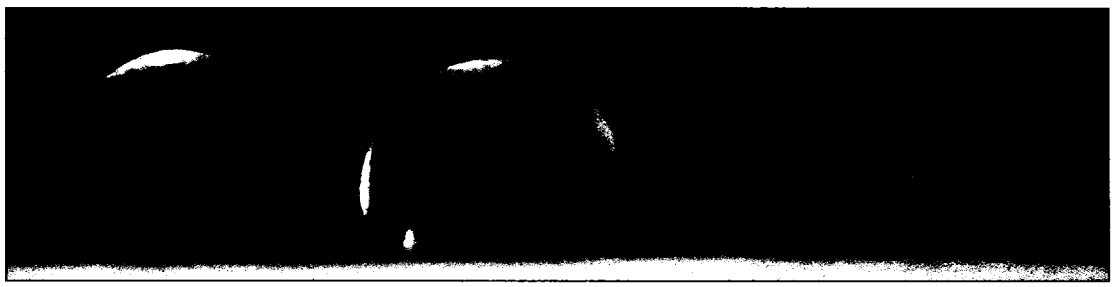

Figure 3.2k: t=105 seconds. Full surface coverage of pure water droplet.

Figure 3.2l: t=180 seconds (2 minutes).

Figure 3.2: Progression of hydrate nucleation and growth on droplets in the presence of kinetic inhibitors.

Surface morphology of the droplets is shown in **Figure 3.3** from experiment 6c immediately after hydrate formation. Subsequent pictures illustrate surface morphology of the droplets both 40 minutes (**Figure 3.4**) and 4 hours (**Figure 3.5**) after all of the droplets had formed hydrate. The hydrate skin becomes noticeably thicker as time progresses and in the case of the AFP droplet (on right) dendrites continue to grow until they fracture under the weight.

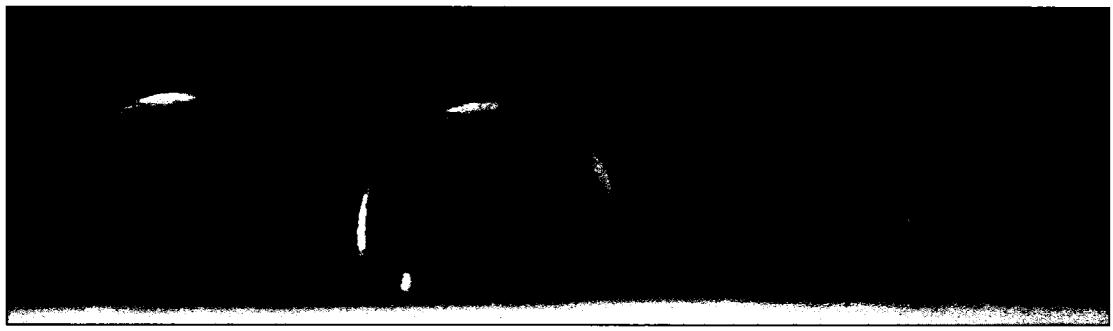

Figure 3.3: Droplets 1 minute after hydrate formation.

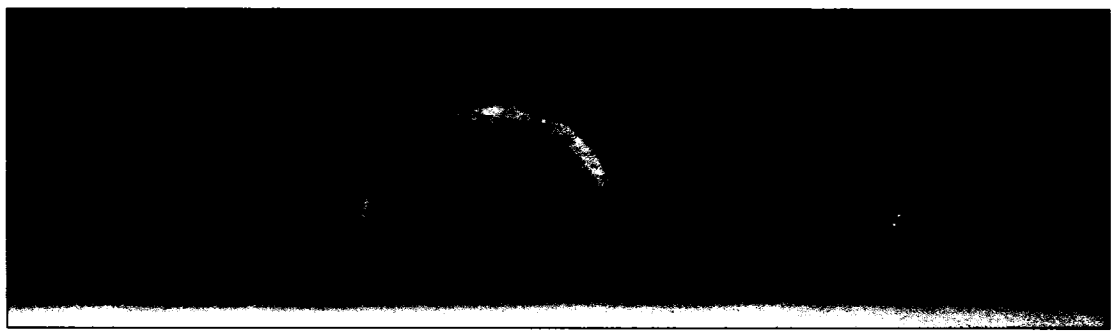

Figure 3.4: Droplets 40 minutes after hydrate formation.

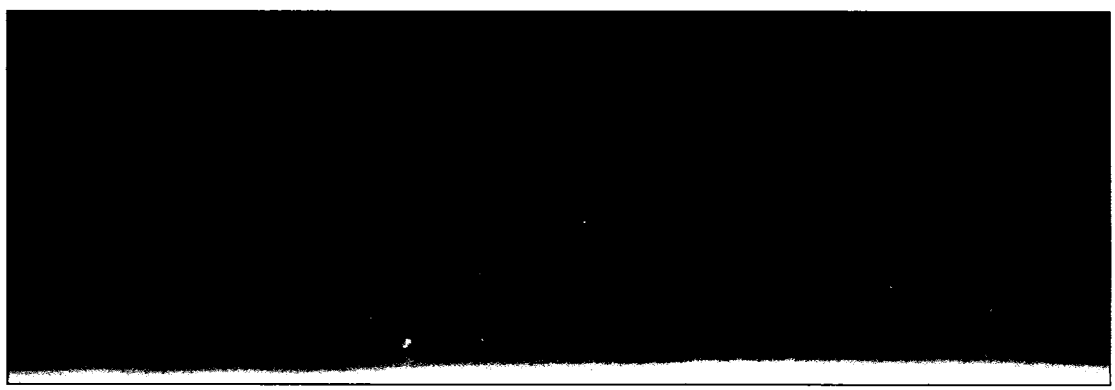

Figure 3.5: Droplets 4 hours after hydrate formation.

All three droplets differed significantly in terms of surface morphology. In experiments with memory, the hydrate skin on the water droplet appeared smooth and shiny as a result of uniform growth. After a prolonged period of time the hydrate skin also seemed thicker than that of the droplets with inhibitors.

The hydrate skin of the poly(VP/VC) droplet was rougher and more translucent than that of the water droplet. Striations were also present in the direction of growth on the droplet. The polymer has been reported to bind to hydrate crystals, preventing growth in the respective plane. The inhibitor does not necessarily fully cover the surface of the droplet or bind to all of the hydrate. Regions where inhibitor is not present will be thicker since growth is not affected and regions where inhibitors are bound to hydrate will be thinner. This explains the rough, translucent morphology that is observed.

The hydrate skin of the AFP droplet is rough, cratered and translucent when compared to that of the water droplet. Similarly to the polymer chains, the protein molecules slow hydrate growth by binding to the crystals, causing uneven growth patterns, as hypothesized with poly(VP/VC). Since the surface of the hydrated AFP droplet is even more translucent than that of the poly(VP/VC) droplet, one can conclude that antifreeze protein is a more effective kinetic inhibitor than the copolymer used.

Another observation made in some experiments during hydrate formation was the deformation of droplets caused by momentum in the direction of growth, particularly on the poly(VP/VC) droplet. As seen in **Figure 3.5**, the poly(VP/VC) droplet is slightly leaning toward the right which is consistent with the direction of growth on that droplet from left to right.

The two kinetic inhibitors studied had a significant effect on methane structure I hydrate morphology. Hydrate formed from pure water droplets resulted in a smooth shiny surface. Hydrate formed from water droplets in the presence of poly(VP/VC) resulted in rough, translucent surface caused by uneven growth patterns. Hydrate formed from water droplets in the presence of AFP resulted in a rough and even more translucent surface than in the presence of the copolymer. This leads us to believe that AFP has a greater inhibiting effect than poly(VP/VC).

3.4 Effect of Kinetic Inhibitors on Hydrate Surface Coverage Time of Droplets

Time of complete surface coverage was measured for each droplet. An example of the progression of surface coverage time is shown in **Figure 3.6** on a poly(VP/VC) droplet from experiment 6c.

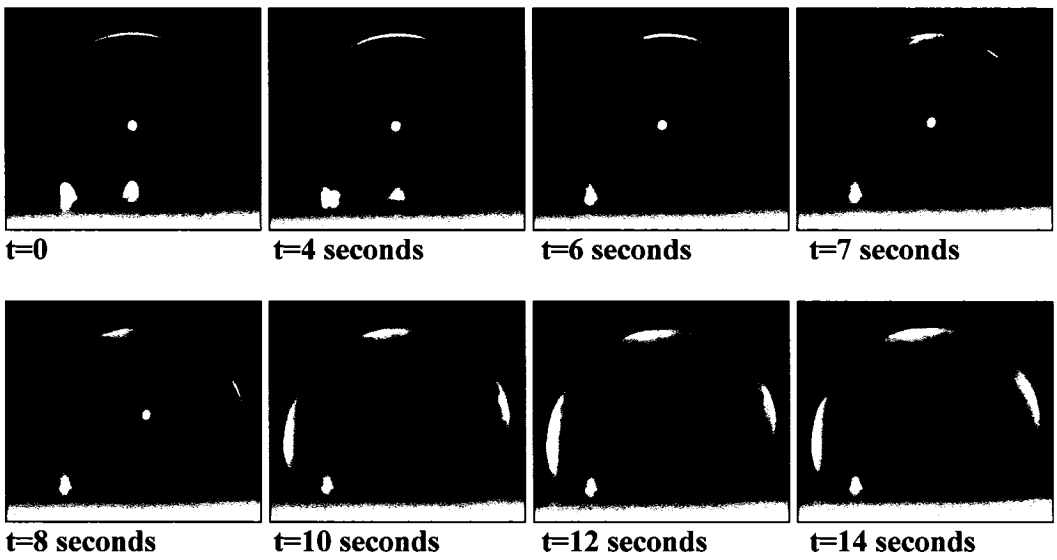

Figure 3.6 Formation time of hydrate skin on a poly(VP/VC) droplet

Average time of surface coverage was measured for all three droplets at pressures of 6500 kPa, 7200 kPa and 10,000 kPa by using the frame rate and frame number. Results could not be included at pressures of 5000 kPa due to a lack of data. The results are shown in **Figure 3.7**.

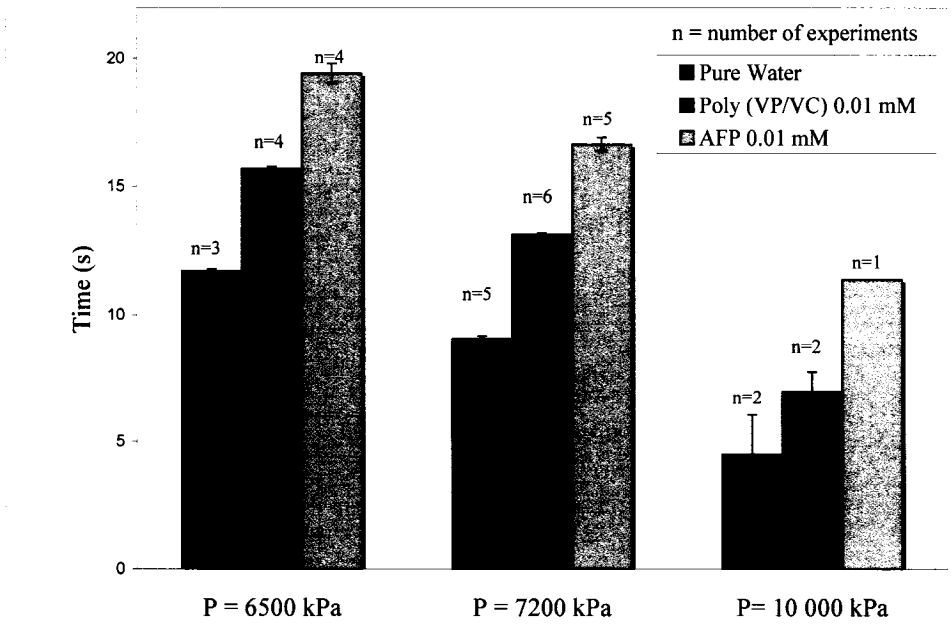

Figure 3.7: Effect of kinetic inhibitors on hydrate surface coverage time of droplet at 275.2 K

Surface coverage time was found to be affected by the presence of kinetic inhibitor, the type of kinetic inhibitor and experimental pressure. At 6500 kPa, average surface coverage time of the water droplet, poly(VP/VC) droplet and AFP droplet were 11.7, 15.7 and 19.4 seconds, respectively. At a higher pressure of 7200 kPa, a decrease in average surface coverage time was observed. They were reported to be 9.1, 13.1 and 16.6 seconds for the water droplet, poly(VP/VC) droplet and AFP droplet, respectively.

At an even higher pressure of 10,000 kPa a similar trend was observed. In summary, surface coverage time of hydrate skin on the pure water droplet was shortest, followed by that of the poly(VP/VC) droplet and finally the AFP droplet. Since surface coverage time is proportional to hydrate crystal growth, the above results concur with previous studies that the kinetic inhibitors studied do indeed slow the rate of hydrate growth (Carver et al., 1996; Eberhardt et al., 1997; Fu et al., 2001; Karaaslan and Parlaktuna, 2002; Lederhos et al., 1996; Lovell and Pakulski, 2003; Monfort et al., 2000; Ohtake et al., 2005; Sakaguchi et al., 2003; Svartaas et al., 2000). It can also be noted from **Figure 3.7** that surface coverage time decreases with increasing pressure. This is because the greater the deviation from the three phase equilibrium pressure the higher the crystal driving force and thus the faster the growth rate.

The observation of hydrate surface coverage time of droplets with and without kinetic inhibitors leads to the conclusion that both antifreeze protein and poly(VP/VC) have inhibiting effects on the rate of methane hydrate growth. Since surface coverage time of antifreeze protein was higher than that of the copolymer at various pressures, it can be concluded that of the two kinetic inhibitors studied, antifreeze protein was the more effective inhibitor.

3.5 Morphology during Decomposition of Hydrate on Pure Water Droplets

Structure I methane hydrate was formed at 275.2 K on three pure water droplets and subsequently decomposed by dropping the pressure below the equilibrium pressure of 3020 kPa, to approximately 2900 kPa. Simultaneous decomposition of the hydrate skin was observed on all three droplets followed by the release of methane gas from the droplets (**Figure 3.8**).

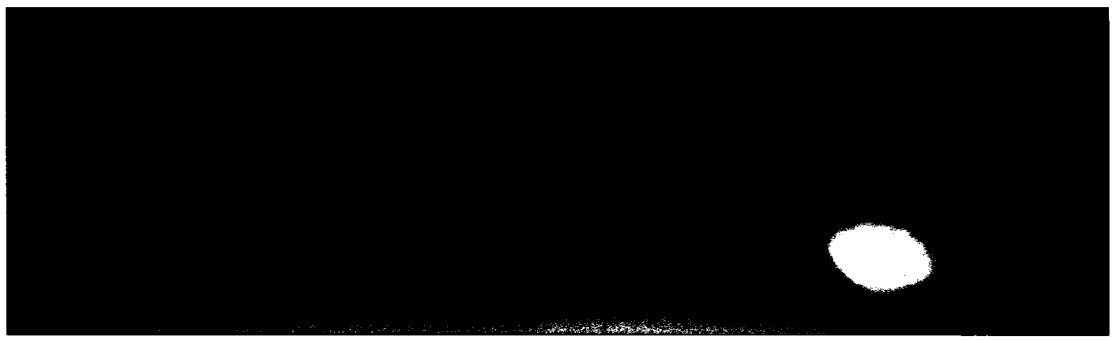

Figure 3.8a: t=0 seconds.

Figure 3.8b: t=15 seconds.

Figure 3.8c: t=30 seconds.

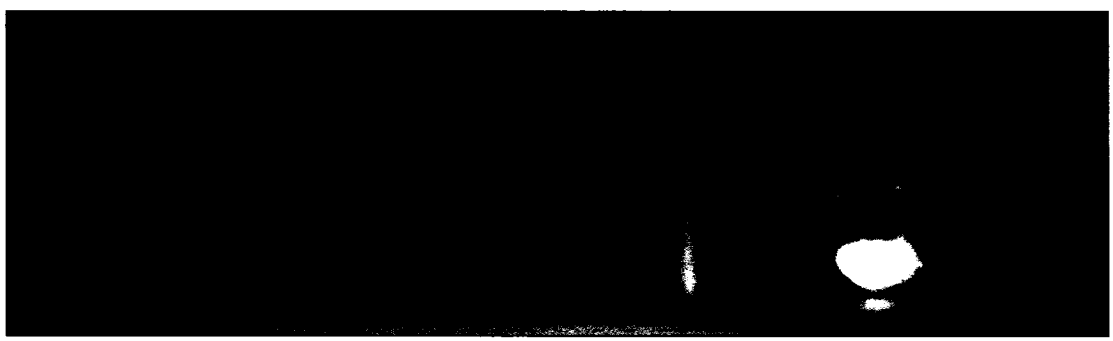

Figure 3.8d: t=45 seconds.

Figure 3.8e: 60 seconds.

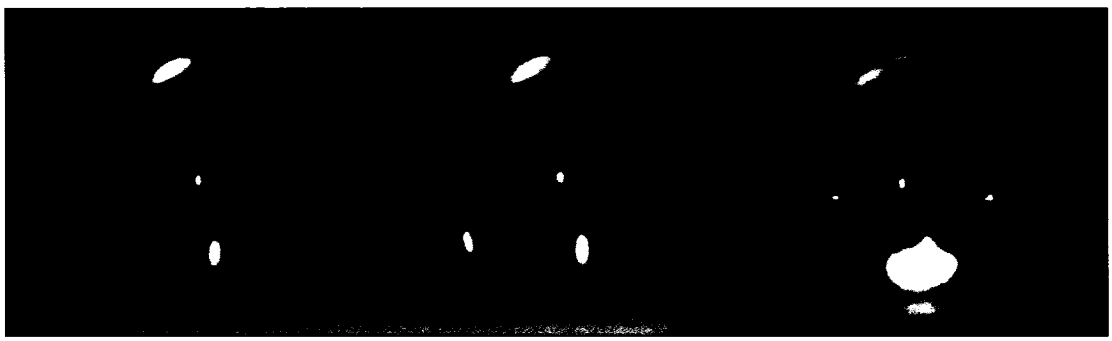

Figure 3.8f: t=2 minutes.

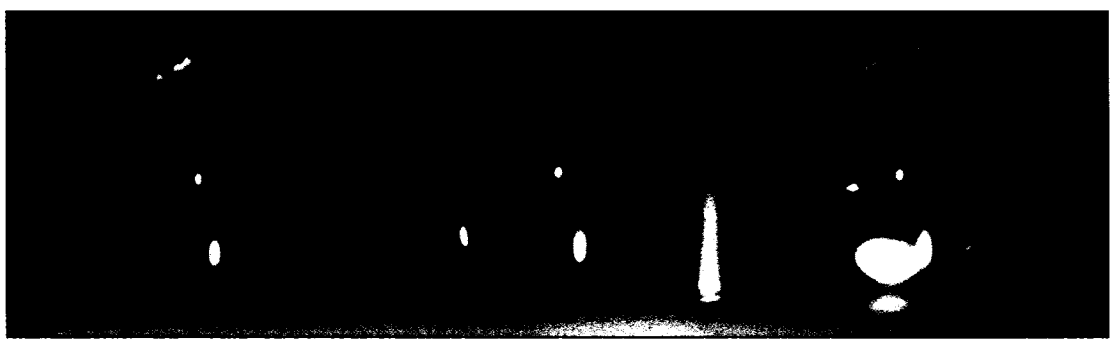

Figure 3.8g: t=3 minutes.

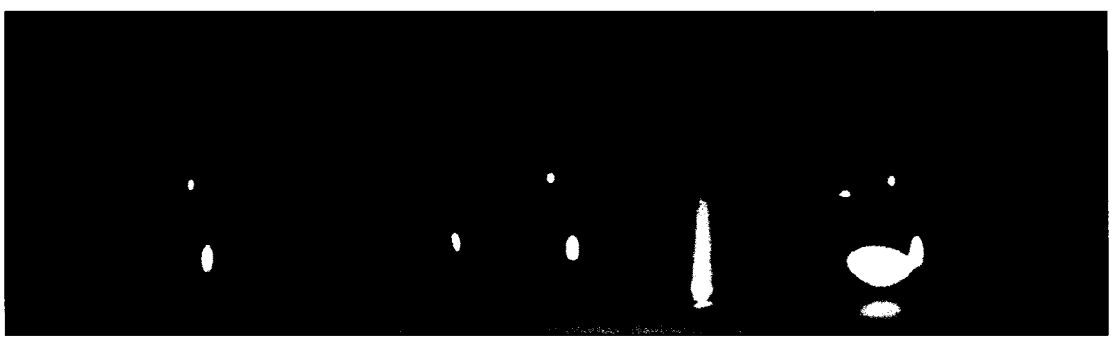

Figure 3.8h: t=4 minutes.

Figure 3.8: Decomposition of three pure water droplets

It can be concluded from **Figure 3.8** that all three droplets decomposed at the same rate in the absence of kinetic inhibitors. The reason for this can be attributed to the similarity in composition and surface morphology of the water droplets to one another.

3.6 Morphology during Decomposition of Hydrate on Water Droplets in the Presence of Kinetic Inhibitors

Hydrate decomposition was achieved by dropping the pressure below the equilibrium pressure of 3020 kPa to approximately 2900 kPa as described in the previous section. Observations made during the decomposition of methane hydrate formed from droplets in the presence of inhibitors were significantly different from those made during decomposition of hydrate formed from pure water. The droplet on the left in **Figure 3.9** is pure water; the droplet in the middle contains 0.01 mM of poly(VP/VC); the droplet on the right contains 0.01 mM of AFP.

Figure 3.9a: t=0 seconds.

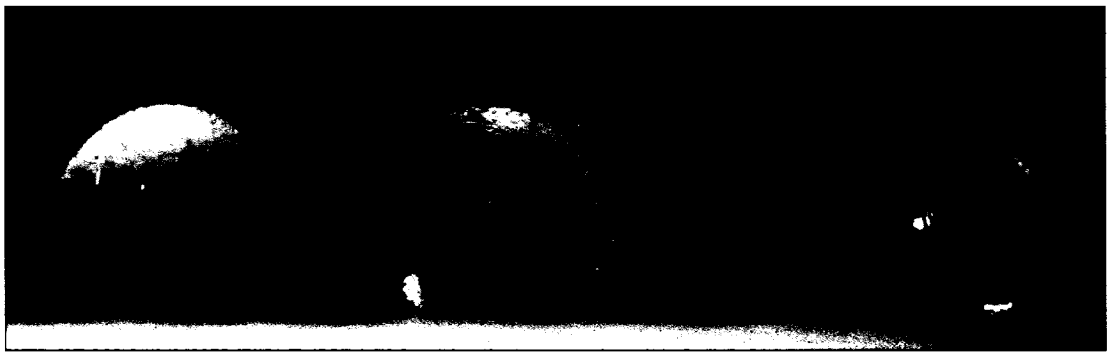

Figure 3.9b: t=30 seconds. Hydrate skin of water droplet decomposing.

Figure 3.9c: t=40 seconds. Dendrites receding on all droplets.

Figure 3.9d: t=50 seconds. Dendrites continuing to recede. Hydrate skin of poly(VP/VC) droplet starting to decompose.

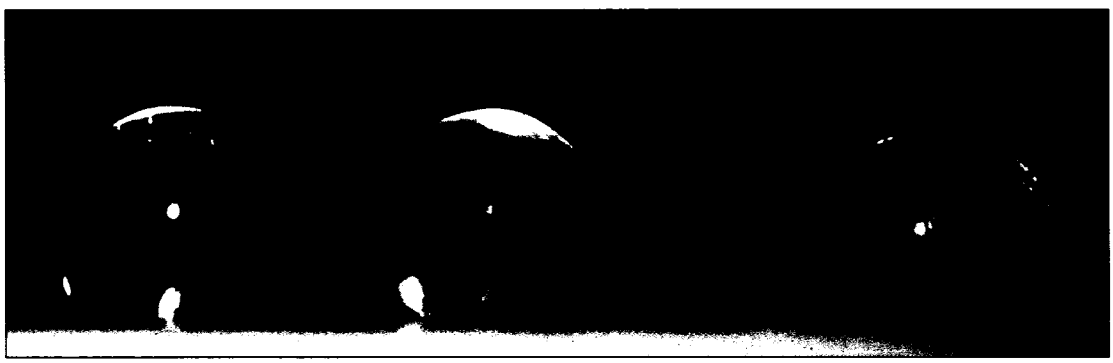

Figure 3.9e: t=90 seconds. Methane bubbles being released from water droplet.

Figure 3.9f: t=2 minutes.

Figure 3.9g: t=3 minutes.

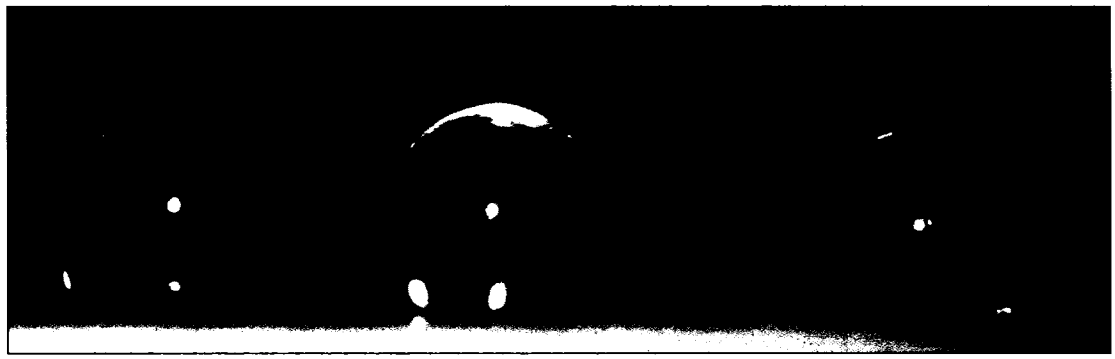

Figure 3.9h: t=3.5 minutes.

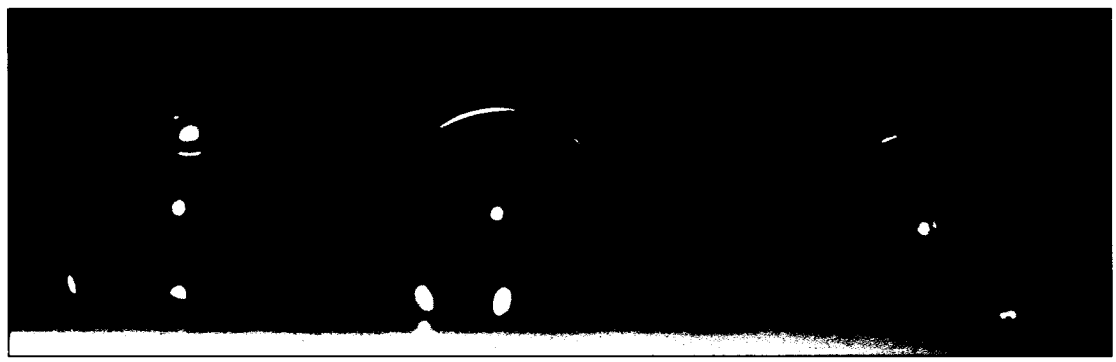

Figure 3.9i: t=4 minutes.

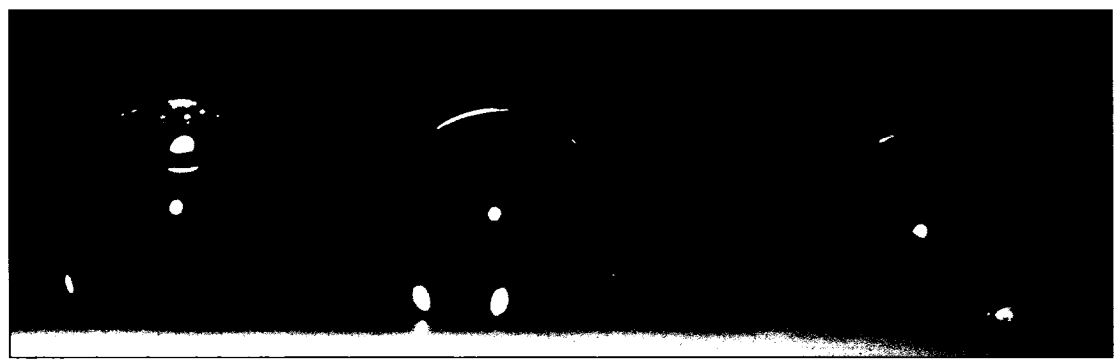

Figure 3.9j: t=5 minutes.

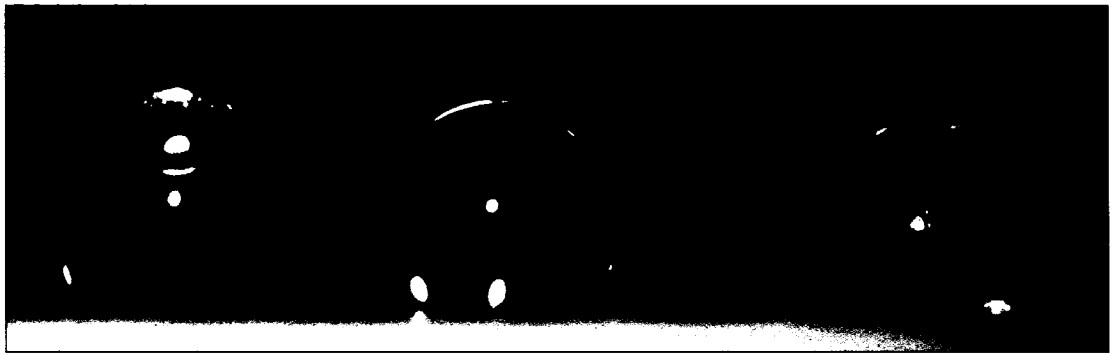

Figure 3.9k: t=6 minutes.

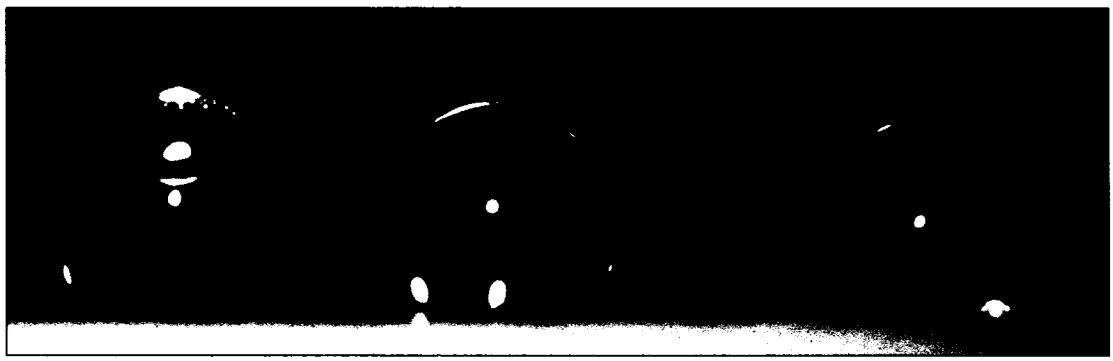

Figure 3.9l: t=7 minutes. Hydrate skin of all droplets fully decomposed. Methane bubbles being released.

Figure 3.9: Decomposition of methane structure I hydrate.

Decomposition of hydrate in the presence of inhibitors was noticeably slower than decomposition of hydrate on the pure water droplet, despite the thicker appearance of the hydrate skin on the water droplet. In all experiments, the hydrate skin on the water droplet decomposed first relative to that of the hydrated droplets containing inhibitors. Decomposition of hydrate on the poly(VP/VC) droplet occurred second, after decomposition of hydrate on the pure water droplet. Decomposition of the AFP droplet occurred last. As explained earlier, during hydrate formation, the polymer or antifreeze protein binds to hydrate crystals, preventing growth. The surface area of hydrate skin exposed is reduced due to the binding of inhibitors. Regions where inhibitors are bound

to hydrate crystals are not subject to the same temperature and pressure conditions as regions where hydrate crystals are free from inhibitor binding. This causes a blanket effect, protecting these particular regions and slowing the rate of decomposition. At later stages of decomposition, the rough surface of the droplets with inhibitors appears to trap methane bubbles and in some cases, preventing their release.

To summarize, the kinetic inhibitors studied slow the rate of decomposition of hydrate skin on droplets. The rate of decomposition of hydrate on the water droplet was fastest. The rate of decomposition of hydrate on the poly(VP/VC) droplet was slower than that on the pure water droplet and finally, the rate of decomposition was slowest on droplets with antifreeze protein.

4 CONCLUSION AND RECOMMENDATIONS

4.1 Conclusions

A high pressure reactor capable of withstanding pressures of up to 20,000 kPa was designed. A set up was then built in order to perform morphology studies on droplets in the presence of kinetic inhibitors. Two kinetic inhibitors were studied. The first was a lactam ring copolymer, a 1:1 molar mixture of polyvinylpyrrolidone (PVP) and polyvinylcaprolactam (PVCap). The second was antifreeze protein obtained from the winter flounder (*pseudopleuronectes americanus*).

Experiments were carried out on droplets without memory at pressures of 7200 kPa and 10,000 kPa. When nucleation occurred, the water droplet formed hydrate first, followed by the AFP droplet and finally the poly(VP/VC) droplet. In some experiments however, nucleation did not occur within 24 hours and the experiments were terminated.

Experiments were carried out on droplets with memory at pressures of 5000 kPa, 6500 kPa, 7200 kPa and 10,000 kPa. There was no evident trend in induction times since nucleation is a stochastic process that is hard to predict. In some experiments, hydrate formed on all droplets within three minutes of each other. This may be the result of a communication effect, a memory effect or a combination of the two. In other experiments, no nucleation occurred within 24 hours.

Some kinetics can be deduced for measuring the elapsed time required for a hydrate film to fully cover the water droplet. The surface coverage time of a hydrate skin on the pure water droplet was the shortest followed by that of the poly(VP/VC) droplet and finally the AFP droplet, confirming that the two kinetic inhibitors studied were in

fact effective at inhibiting hydrate growth. Since hydrate growth, unlike nucleation, can reliably be measured we can definitively conclude that AFP has a greater kinetic inhibiting effect on hydrate growth than poly(VP/VC). It was also observed that with increasing pressure, surface coverage time decreased.

During hydrate decomposition, it was observed in all experiments that the water droplet decomposed first followed by the poly(VP/VC) droplet and the AFP droplet. It is proposed that binding of the polymer chains and protein molecules to hydrate crystals in various regions causes a blanket effect, protecting these regions and slowing the rate of decomposition.

4.2 Recommendations for Future Work

There are several important points related to morphology studies to be addressed in future work and they are as follows:

1) To perform the experiments at various temperatures in order to observe the effect of temperature on hydrate surface coverage time, crystal morphology and effectiveness of the kinetic inhibitors.
2) To quantify hydrate growth of a plane film at a stagnant gas-liquid interface and to develop a relationship between growth and film thickness. This would be achieved by correlating the number of moles consumed of hydrate forming gas with the distance traveled by the front of the hydrate film into the liquid phase.

3) To quantify hydrate growth of a film on a droplet and to develop a relationship between radial growth and film thickness using similar correlations mentioned above.

4) To model the relationships developed between hydrate growth and film thickness and to compare results of growth on a stagnant film and on a droplet.

5) To observe the effect of kinetic inhibitors on hydrate growth at a plane gas-liquid interface and on a droplet and to quantify this growth.

REFERENCES

Aya, I., K. Yamane, and N. Yamada, 1993, Stability of clathrate-hydrate of carbon dioxide in highly pressurized water: Nippon Kikai Gakkai Ronbunshu, B-hen, v. 59, p. 1210-15.

Bylov, M., and P. Rasmussen, 1996, A new technique for measuring gas hydrate kinetics: International Conference on Natural Gas Hydrates, 2nd, Toulouse,June 2-6, 1996, p. 259-266.

Carver, T. J., M. G. B. Drew, and P. M. Rodger, 1996, Characterization of the {111} growth planes of a type II gas hydrate and study of the mechanism of kinetic inhibition by poly(vinylpyrrolidone): Journal of the Chemical Society, Faraday Transactions, v. 92, p. 5029-5033.

Chapsky, L., and B. Rubinsky, 1997, Kinetics of antifreeze protein-induced ice growth inhibition: FEBS Letters, v. 412, p. 241-244.

Davies, P. L., J. Baardsnes, M. J. Kuiper, and V. K. Walker, 2002, Structure and function of antifreeze proteins: Philosophical Transactions of the Royal Society of London, Series B: Biological Sciences, v. 357, p. 927-935.

De Graauw, J., and J. J. Rutten, 1970, Mechanism and the rate of hydrate formation: Proc. Int. Symp. Fresh Water Sea, 3rd, v. 3, p. 103-16.

DeVries, A. L., and D. E. Wohlschlag, 1969, Freezing resistance in some Antarctic fishes: Science, v. 163, p. 1073-5.

Du, N., X. Y. Liu, and C. L. Hew, 2003, Ice Nucleation Inhibition: mechanism of antifreeze by antifreeze protein: Journal of Biological Chemistry, v. 278, p. 36000-36004.

Eberhardt, E., J. Froemmel, and A. Hase, 1997, Inhibition of natural gas hydrates with kinetic inhibitors: DGMK Tagungsbericht, v. 9706, p. 95-105.

Englezos, P., 1993, Clathrate hydrates: Industrial & Engineering Chemistry Research, v. 32, p. 1251-74.

Englezos, P., 1996, Nucleation and growth of gas hydrate crystals in relation to \"kinetic inhibition\": Revue de l'Institut Francais du Petrole, v. 51, p. 789-795.

Englezos, P., N. Kalogerakis, P. D. Dholabhai, and P. R. Bishnoi, 1987, Kinetics of formation of methane and ethane gas hydrates: Chemical Engineering Science, v. 42, p. 2647-58.

Fu, S. B., L. M. Cenegy, and C. S. Neff, 2001, A summary of successful field applications of a kinetic hydrate inhibitor: SPE International Symposium on Oilfield Chemistry, Conference Proceedings, Houston, TX, United States, Feb. 13-16, 2001, p. 329-336.

Glew, D. N., and M. L. Haggett, 1968a, Kinetics of formation of ethylene oxide hydrate. I. Experimental method and congruent solutions: Canadian Journal of Chemistry, v. 46, p. 3857-65.

Glew, D. N., and M. L. Haggett, 1968b, Kinetics of formation of ethylene oxide hydrate. II. Incongruent solutions and discussion: Canadian Journal of Chemistry, v. 46, p. 3867-77.

Hammerschmidt, E. G., 1934, Formation of gas hydrates in natural gas transmission lines: Journal of Industrial and Engineering Chemistry (Washington, D. C.), v. 26, p. 851-5.

Huo, Z., E. Freer, M. Lamar, B. Sannigrahi, D. M. Knauss, and E. D. Sloan, 2001, Hydrate plug prevention by anti-agglomeration: Chemical Engineering Science, v. 56, p. 4979-4991.

Kamath, V. A., G. D. Holder, and P. F. Angert, 1984, Three phase interfacial heat transfer during the dissociation of propane hydrates: Chemical Engineering Science, v. 39, p. 1435-42.

Karaaslan, U., and M. Parlaktuna, 2002, Kinetic inhibition of methane hydrate by polymers: Preprints of Symposia - American Chemical Society, Division of Fuel Chemistry, v. 47, p. 355-358.

Kato, M. I., T.; Mori, Y.H., 2000, Drop Formation Behaviour of a Hydrate-Forming Liquid in a Water Stream: J. Fluid Mechanics, v. 414, p. 367.

Kim, H. C., P. R. Bishnoi, R. A. Heidemann, and S. S. H. Rizvi, 1987, Kinetics of methane hydrate decomposition: Chemical Engineering Science, v. 42, p. 1645-53.

Kubota, N., M. Yokota, and J. W. Mullin, 1997, Supersaturation dependence of crystal growth in solutions in the presence of impurity: Journal of Crystal Growth, v. 182, p. 86-94.

Larsen, R., T. Makogon, C. Knight, and S. E. Dendy, 1996, The influence of kinetic inhibitors on the morphology of structure I and II clathrate hydrates: International Conference on Natural Gas Hydrates, 2nd, Toulouse,June 2-6, 1996, p. 163-170.

Lederhos, J. P., J. P. Long, A. Sum, R. L. Christiansen, and E. D. Sloan, Jr., 1996, Effective kinetic inhibitors for natural gas hydrates: Chemical Engineering Science, v. 51, p. 1221-9.

Lovell, D., and M. Pakulski, 2003, Two low-dosage hydrate inhibitors: JPT, Journal of Petroleum Technology, v. 55, p. 65-68.

Maini, B. B., and P. R. Bishnoi, 1981, Experimental investigation of hydrate formation behavior of a natural gas bubble in a simulated deep sea environment: Chemical Engineering Science, v. 36, p. 183-9.

Makogon, Y., and Editor, 1997, Hydrates of Hydrocarbons, 400 pp p.

Makogon, Y., Treblin, FA, Trofimuk, AA, Tsarev, VP, Chersky, NV, 1972, Detection of a Pool of Natural Gas in Solid (Hydrate Gas) State: Dokl. Acad. Sci. USSR-Earth Sci., v. 196, p. 197-200.

Makogon, Y. F., 1994, Russia's contribution to the study of gas hydrates: Annals of the New York Academy of Sciences, v. 715, p. 119-45.

Monfort, J. P., L. Jussaume, T. El Hafaia, and J. P. Canselier, 2000, Kinetics of gas hydrates formation and tests of efficiency of kinetic inhibitors Experimental and theoretical approaches: Annals of the New York Academy of Sciences, v. 912, p. 753-765.

Monfort, J. P., and A. Nzihou, 1993, Light scattering kinetics study of cyclopropane hydrate growth: Journal of Crystal Growth, v. 128, p. 1182-6.

Natarajan, V., P. R. Bishnoi, and N. Kalogerakis, 1994, Induction phenomena in gas hydrate nucleation: Chemical Engineering Science, v. 49, p. 2075-87.

Nerheim, A. R., M. T. Svartaas, and E. K. Samuelsen, 1992, Investigation of Hydrate Kinetics in the Nucleation and Early Growth Phase by Laser Light Scattering: Proceedings of the Second International Offshore and Polar Engineering Conference.

Nguyen, D. H., M. E. Colvin, Y. Yeh, R. E. Feeney, and W. H. Fink, 2004, Intermolecular interaction studies of winter flounder antifreeze protein reveal the existence of thermally accessible binding state: Biopolymers, v. 75, p. 109-117.

Nojima, K., and Y. H. Mori, 1994, Clathrate hydrate formation on single refrigerant vapor bubbles released into water: An observational study: Heat Transfer 1994, Proc. Int. Heat Transfer Conf., 10th, v. 3, p. 377-82.

Nojima, K. M., Y.H., 1994: Proc. Int. Heat Transfer Conf., 10th, p. 377-382.

Ohmura, R., T. Shigetomi, and Y. H. Mori, 1999, Formation, growth and dissociation of clathrate hydrate crystals in liquid water in contact with a hydrophobic hydrate-forming liquid: Journal of Crystal Growth, v. 196, p. 164-173.

Ohtake, M., Y. Yamamoto, T. Kawamura, A. Wakisaka, W. F. De Souza, and A. M. V. De Freitas, 2005, Clustering Structure of Aqueous Solution of Kinetic Inhibitor of Gas Hydrates: Journal of Physical Chemistry B, v. 109, p. 16879-16885.

Parent, J. S., 1993, Investigation into the Nucleation Behaviour of Clathrate Hydrates of Natural Gas Components: M. Sc. Thesis thesis, University of Calgary.

Parent, J. S., and P. R. Bishnoi, 1996, The nucleation behavior of methane gas hydrates: Chemical Engineering Communications, v. 144, p. 51-64.

Raymond, J. A., and A. L. DeVries, 1977, Adsorption inhibition as a mechanism of freezing resistance in polar fishes: Proceedings of the National Academy of Sciences of the United States of America, v. 74, p. 2589-93.

Sakaguchi, H., R. Ohmura, and Y. H. Mori, 2003, Effects of kinetic inhibitors on the formation and growth of hydrate crystals at a liquid-liquid interface: Journal of Crystal Growth, v. 247, p. 631-641.

Servio, P., 2002, Kinetic, equilibrium and morphology studies of hydrate-forming systems, 128 pp p.

Servio, P., and P. Englezos, 2003, Morphology of methane and carbon dioxide hydrates formed from water droplets: AIChE Journal, v. 49, p. 269-276.

Shindo, Y., P. C. Lund, Y. Fujioka, and H. Komiyama, 1993, Kinetics of formation of carbon dioxide hydrate: Energy Conversion and Management, v. 34, p. 1073-9.

Skovborg, P., H. J. Ng, P. Rasmussen, and U. Mohn, 1993, Measurement of induction times for the formation of methane and ethane gas hydrates: Chemical Engineering Science, v. 48, p. 445-53.

Sloan, E. D., 1990, Natural gas hydrate phase equilibria and kinetics: understanding the state-of-the-art: Revue de l'Institut Francais du Petrole, v. 45, p. 245-66.

Sloan, E. D., Jr., 1998a, Clathrate Hydrates of Natural Gases: New York, Marcel Dekker, Inc.

Sloan, E. D., Jr., 1998b, Gas Hydrates: Review of Physical/Chemical Properties: Energy & Fuels, v. 12, p. 191-196.

Sloan, E. D., Jr., and F. Fleyfel, 1991, A molecular mechanism for gas hydrate nucleation from ice: AIChE Journal, v. 37, p. 1281-92.

Strom, C. S., X. Y. Liu, and Z. Jia, 2004, Antifreeze Protein-induced Morphological Modification Mechanisms Linked to Ice Binding Surface: Journal of Biological Chemistry, v. 279, p. 32407-32417.

Sugaya, M., and Y. H. Mori, 1996, Behavior of clathrate hydrate formation at the boundary of liquid water and a fluorocarbon in liquid or vapor state: Chemical Engineering Science, v. 51, p. 3505-3517.

Svartaas, T. M., M. A. Kelland, and L. Dybvik, 2000, Experiments related to the performance of gas hydrate kinetic inhibitors: Annals of the New York Academy of Sciences, v. 912, p. 744-752.

Takeya, S., 1999, Experimental Studies on Formation Mechanisms of Clathrate Hydrate Crystals: Doctoral Dissertation thesis, Hokkaido University.

Taylor, F. W., 1991, The greenhouse effect and climate change: Reports on Progress in Physics, v. 54, p. 881-918.

Topham, D. R., 1984, The formation of gas hydrates on bubbles of hydrocarbon gases rising in seawater: Chemical Engineering Science, v. 39, p. 821-8.

Vysniauskas, A., and P. R. Bishnoi, 1983, Thermodynamics and kinetics of gas hydrate formation: Nat. Gas Hydrates, p. 35-48.

Wilson, P. W., 1993, Explaining Thermal Hysteresis by the Kelvin Effect: Cryo-Letters, v. 14, p. 31-36.

Xie, Y., K. Guo, D. Liang, S. Fan, and J. Gu, 2005, Gas hydrate growth morphology outside of horizontal heat transfer tube: Journal of Crystal Growth, v. 276, p. 253-264.